

The DECam MAGIC Survey: A Wide-field Photometric Metallicity Study of the Sculptor Dwarf Spheroidal Galaxy

F. O. BARBOSA ¹, A. CHITI ^{2,3}, G. LIMBERG ³, A. B. PACE ⁴, W. CERNY ⁵, S. ROSSI ¹, J. L. CARLIN ⁶,
G. S. STRINGFELLOW ⁷, V. M. PLACCO ⁸, K. ATZBERGER ⁴, J. A. CARBALLO-BELLO ⁹, A. CHATURVEDI ¹⁰,
Y. CHOI ⁸, D. CRNOJEVIĆ ¹¹, A. DRLICA-WAGNER ^{12,3,2,13}, A. P. JI ², N. KALLIVAYALIL ⁴,
C. E. MARTÍNEZ-VÁZQUEZ ¹⁴, G. E. MEDINA ^{15,16}, N. E. D. NOËL ¹⁰, D. J. SAND ¹⁷, A. K. VIVAS ¹⁸,
C. R. BOM ¹⁹, P. S. FERGUSON ²⁰, B. MUTLU-PAKDIL ²¹, M. NAVABI ¹⁰, A. H. RILEY ²², J. D. SAKOWSKA ^{10,23},
A. ZENTENO ¹⁸

(MAGIC & DELVE COLLABORATIONS)

- ¹Universidade de São Paulo, Instituto de Astronomia, Geofísica e Ciências Atmosféricas, Departamento de Astronomia, SP 05508-090, São Paulo, Brasil
- ²Department of Astronomy & Astrophysics, University of Chicago, 5640 S. Ellis Avenue, Chicago, IL 60637, USA
- ³Kavli Institute for Cosmological Physics, University of Chicago, 5640 S. Ellis Avenue, Chicago, IL 60637, USA
- ⁴Department of Astronomy, University of Virginia, 530 McCormick Road, Charlottesville, VA 22904, USA
- ⁵Department of Astronomy, Yale University, New Haven, CT 06520, USA
- ⁶Rubin Observatory/AURA, 950 North Cherry Avenue, Tucson, AZ, 85719, USA
- ⁷Center for Astrophysics and Space Astronomy, University of Colorado Boulder, Boulder, CO 80309, USA
- ⁸NSF NOIRLab, 950 N. Cherry Ave., Tucson, AZ 85719, USA
- ⁹Instituto de Alta Investigación, Universidad de Tarapacá, Casilla 7D, Arica, Chile
- ¹⁰Department of Physics, University of Surrey, Guildford GU2 7XH, UK
- ¹¹Department of Physics & Astronomy, University of Tampa, 401 West Kennedy Boulevard, Tampa, FL 33606, USA
- ¹²Fermi National Accelerator Laboratory, P.O. Box 500, Batavia, IL 60510, USA
- ¹³NSF-Simons AI Institute for the Sky (SkAI), 172 E. Chestnut St., Chicago, IL 60611, USA
- ¹⁴NSF NOIRLab, 670 N. A'ohoku Place, Hilo, Hawai'i, 96720, USA
- ¹⁵David A. Dunlap Department of Astronomy & Astrophysics, University of Toronto, 50 St George Street, Toronto ON M5S 3H4, Canada
- ¹⁶Dunlap Institute for Astronomy & Astrophysics, University of Toronto, 50 St George Street, Toronto, ON M5S 3H4, Canada
- ¹⁷Department of Astronomy/Steward Observatory, 933 North Cherry Avenue, Room N204, Tucson, AZ 85721-0065, USA
- ¹⁸Cerro Tololo Inter-American Observatory/NSF NOIRLab, Casilla 603, La Serena, Chile
- ¹⁹Centro Brasileiro de Pesquisas Físicas, Rua Dr. Xavier Sigaud 150, 22290-180 Rio de Janeiro, RJ, Brazil
- ²⁰DiRAC Institute, Department of Astronomy, University of Washington, 3910 15th Ave NE, Seattle, WA, 98195, USA
- ²¹Department of Physics and Astronomy, Dartmouth College, Hanover, NH 03755, USA
- ²²Institute for Computational Cosmology, Department of Physics, Durham University, South Road, Durham DH1 3LE, UK
- ²³Instituto de Astrofísica de Andalucía, CSIC, Glorieta de la Astronomía, E-18080 Granada, Spain

ABSTRACT

The metallicity distribution function and internal chemical variations of a galaxy are fundamental to understand its formation and assembly history. In this work, we analyze photometric metallicities for 3883 stars over seven half-light radii (r_h) in the Sculptor dwarf spheroidal (Scl dSph) galaxy, using new narrow-band imaging data from the Mapping the Ancient Galaxy in CaHK (MAGIC) survey conducted with the Dark Energy Camera (DECam) at the 4-m Blanco Telescope. This work demonstrates the scientific potential of MAGIC using the Scl dSph galaxy, one of the most well-studied satellites of the Milky Way. Our sample ranges from $[\text{Fe}/\text{H}] \approx -4.0$ to $[\text{Fe}/\text{H}] \approx -0.6$, includes six extremely metal-poor candidates ($[\text{Fe}/\text{H}] \leq -3.0$) without previous spectroscopic observations, and is almost three times larger than the largest spectroscopic metallicity dataset in the Scl dSph. Our spatially unbiased

sample of metallicities provides a more accurate representation of the metallicity distribution function, revealing a more metal-rich peak than observed in the most recent spectroscopic sample. It also reveals a break in the metallicity gradient, with a strong change in the slope: from -3.35 ± 0.18 dex deg $^{-1}$ for stars inside ~ 1 r $_h$ to -0.56 ± 0.26 dex deg $^{-1}$ for the outer part of the Scl dSph. Our study demonstrates that combining photometric metallicity analysis with the wide field of view of DECam offers an efficient and unbiased approach for studying the stellar populations of dwarf galaxies in the Local Group.

Keywords: Dwarf galaxies (416), Dwarf spheroidal galaxies (420), Metallicity (1031)

1. INTRODUCTION

According to the Λ Cold Dark Matter paradigm, massive galaxies are formed by the aggregation of smaller systems (Searle & Zinn 1978, Faber & Gallagher 1979, White & Frenk 1991, Kauffmann et al. 1993, Johnston 1998, Springel et al. 2006). There is plenty of evidence, from kinematic and chemical properties, to suggest that the halo of the Milky Way is composed of a diverse range of disrupted systems (see reviews by Helmi 2008, Belokurov 2013, Helmi 2020, and Deason & Belokurov 2024). These disrupted systems were once bound dwarf galaxies, similar to the satellites observed today in the Local Group. Therefore, the study of present-day surviving satellites can be used to study the formation and evolution of systems that form galactic halos, and also test galaxy formation processes in the low-mass regime.

To understand the formation history and evolution of such systems, the investigation of the chemical composition of individual member stars is necessary. Particularly, stellar metallicity distribution functions (MDFs) are useful to shed light on the mechanisms that shape the chemical evolution of galaxies (Lai et al. 2011, Kirby et al. 2011, 2015). To ensure an accurate inference of these properties through fitting analytic chemical evolution models (e.g., Weinberg et al. 2017, Sandford et al. 2024), it is crucial to analyze well-sampled MDFs. Robust samples not only permit obtaining a more reliable fit, but also allow for the discrimination between different models.

Unfortunately, acquiring spectra for a large number of stars in dwarf galaxies is still a challenge. Measurements of iron lines require medium/high-resolution spectroscopy ($R > 10,000$), which means a considerable amount of time (up to a few hours per object) observing targeted stars in systems as distant as the Milky Way’s classical satellites (beyond 70 kpc; McConnachie 2012, Pace 2024). The first spectroscopic studies observed less than a dozen stars (e.g., Bonifacio et al. 2000, Shetrone et al. 2001). Following works, especially those with multi-object observations, increased the number of high-resolution spectra obtained to tens (e.g., Monaco et al. 2005, Koch et al. 2008, Battaglia et al. 2008, Lardo

et al. 2016). Still, the current samples are generally limited to a few hundreds of stars for not even a handful of dwarf spheroidal galaxies (e.g., Sextans, Carina, Sculptor, Draco; Kirby et al. 2009, Walker et al. 2009, 2023).

To overcome this limitation, we can use photometric metallicities derived from narrow-band filters centered around metallicity-sensitive features of stellar spectra. Although this technique is less precise than spectroscopic metallicities, it has proved to be a valuable tool for estimating metallicities for larger samples of stars in dwarf galaxies with a higher efficiency (Longeard et al. 2018, 2020, Chiti et al. 2020, Vitali et al. 2022, Fu et al. 2022, 2023, 2024a,b, Pan et al. 2025). The Ca II H and K lines are the strongest metal lines in a stellar spectrum (Beers et al. 1999). Their strength can thus be measured photometrically with a narrow filter around ~ 3950 Å (hereafter referred to as CaHK filter). At fixed stellar parameters (e.g., effective temperature, surface gravity), a smaller observed flux on the CaHK filter indicates higher element abundances, as more metal-rich stars ought to have stronger Ca II absorption lines.

The effectiveness of CaHK observations has been demonstrated in several previous works. Spectroscopic programs, such as the HK (Beers et al. 1985, Beers et al. 1992) and the Hamburg/ESO (Frebel et al. 2006, Christlieb et al. 2008) surveys, used the Ca II K line to identify metal-poor candidates (see Limberg et al. 2021). It has also been used in photometric studies, such as Anthony-Twarog et al. (1991), that introduced the Ca filter into the *uvby* system to improve the loss of sensitivity below $[\text{Fe}/\text{H}] = -2$ in previous metallicity indices. More recently, the SkyMapper Southern Sky Survey (Keller et al. 2007) and the Pristine survey (Starkenburg et al. 2017) have achieved significant results in the search for metal-poor stars in the Milky Way using metallicity-sensitive filters. The former introduced the *v* filter, which encompasses the Ca II lines, while the latter employs a narrowband filter centered on the Ca II K line. These advances enabled the identification of a few hundred extremely metal-poor stars and have contributed to the characterization of metal-poor stellar systems, such as ultra-faint dwarf galaxies (e.g., Keller

et al. 2014, Youakim et al. 2017, Aguado et al. 2019, da Costa et al. 2019, Chiti et al. 2020, Yong et al. 2021, Longeard et al. 2022). Moreover, the potential of photometric metallicities was explored to estimate metallicity gradients for Milky Way satellites (Han et al. 2020) using Subaru/Suprime-Cam (Aihara et al. 2018), and for two M31 satellites with the Hubble Space Telescope (Fu et al. 2024b), which could not be done with ground-based spectroscopy. Ongoing narrow-band surveys, such as the Southern Photometric Local Universe Survey (SPLUS; Mendes de Oliveira et al. 2019), Javalambre Photometric Local Universe Survey (J-PLUS; Cenarro et al. 2019), and Javalambre-Physics of the Accelerating Universe Astrophysical Survey (J-PAS; Bonoli et al. 2021) are also poised to obtain photometric metallicities in dwarf galaxies for samples of thousands of stars.

The present work explores data from a new photometric CaHK survey, the Mapping the Ancient Galaxy in CaHK (MAGIC; PI: Anirudh Chiti), conducted with the Dark Energy Camera (DECam; Flaughner et al. 2015), on the Victor Blanco 4-m telescope at Cerro Tololo Inter-American Observatory, in Chile, as part of the DECam Local Volume Exploration Survey (DELVE; Drlica-Wagner et al. 2021). In particular, we analyze data for the Sculptor dwarf spheroidal galaxy (Scl dSph), one of the most extensively studied dwarf galaxies in the Local Group, providing numerous spectroscopic studies for comparison (e.g., Kirby et al. 2009, Simon et al. 2015, Chiti et al. 2018, Hill et al. 2019, de los Reyes et al. 2022, Walker et al. 2023, Tang et al. 2023, Tolstoy et al. 2023). Its location is especially suitable for spectroscopic and photometric studies. It is found in the direction of the Galactic pole ($b \sim -83^\circ$), less susceptible to the Galactic extinction, and is close to the Milky Way in comparison to other classical dwarf satellites (heliocentric distance of 83.9 ± 0.5 kpc; Martínez-Vázquez et al. 2015, Pace et al. 2022).

In the first detailed study of Scl dSph’s star formation history, de Boer et al. (2012) suggested an extended star formation period lasting approximately 6–7 Gyr, a range supported by later studies (Martínez-Vázquez et al. 2016, Savino et al. 2018). More recent works, however, report a shorter period of star formation, between 0.9–2.2 Gyr (Weisz et al. 2014, Vincenzo et al. 2016, Bettinelli et al. 2019, de los Reyes et al. 2022). Despite the proposed brief period of star formation, two distinct chemo-dynamical populations characterize it. The central region is dominated by younger, more metal-rich stars with lower velocity dispersion, whereas the more metal-poor population extends from the inner to the outer regions and exhibits higher velocity dispersion (Tolstoy et al. 2004, Arroyo-Polonio et al. 2024). Re-

cently, a third, even lower-metallicity, population was potentially identified with both chemistry and kinematics (Arroyo-Polonio et al. 2024). These updates highlight the importance of systematic, large chemodynamic studies of the Scl dSph, and dSphs more broadly, to understand the processes that shape galaxy formation at the low mass end.

The aim of this paper is to analyze chemical properties of the Scl dSph with the largest metallicity sample to date, while also testing the validity of wide-field photometric metallicities from the new MAGIC photometric survey. Considering all the properties of the Scl dSph that earned it the status of a “textbook dSph galaxy” (Hill et al. 2019), we choose it as the test case to validate our photometric metallicities. Until recently, only 12 members with $[\text{Fe}/\text{H}] < -2.5$ were known (Sestito et al. 2023). This number has increased to 74 with the latest analysis of Very Large Telescope (VLT) data by Tolstoy et al. (2023). Our sample doubles the number of members of this previous work, with about 20 of them being extremely metal-poor (EMP; $[\text{Fe}/\text{H}] < -3$). We show that the photometric metallicities are reliable, potentially reaching $[\text{Fe}/\text{H}]$ as low as -4.0 dex, and they allow us to re-derive the MDF and the metallicity gradient of the Scl dSph. This study demonstrates the power of MAGIC survey in providing a more complete and spatially unbiased metallicity sample for dwarf galaxies in the Local Group.

This work is organized as follows. We describe briefly the catalogues used in Section 2. The method implemented to derive the metallicities and the member selection are presented in Section 3. In Section 4, we evaluate the performance of the photometric metallicities by comparison with previous spectroscopic works. The implications of the new sample for the characterization of the Scl dSph are discussed in Section 5. Finally, we summarize our results in Section 6.

2. DATA

Our photometric dataset combines the DECam broadband data from DELVE and the new narrow-band CaHK observations from MAGIC. We describe each of these components briefly below.

2.1. The MAGIC Survey

The MAGIC survey (Chiti et al. in prep.) provides narrow-band photometry using a CaHK filter on DECam. The new filter, designated as N395, has a central wavelength of 3952 Å, a bandpass of 10 nm, and a “top hat” transmission profile. It was designed to encompass the Ca II H and K lines at 3968.5 Å and 3933.7 Å, respectively, replicating similar filters used for previous

narrow-band metallicity studies (e.g., Pristine survey; Starkenburg et al. 2017). The measured flux through this filter can be combined with DELVE broad-band observations to infer the metallicities for stars over the wide-field observed by the DECam. MAGIC aims to cover at least $\sim 5,500 \text{ deg}^2$ of the southern sky, including a high number of known Milky Way satellites, being a powerful tool for investigating the MDFs of both the Milky Way and its dwarf satellite galaxies. At this stage, MAGIC has covered $\sim 1,500 \text{ deg}^2$ and data collection is ongoing.

MAGIC will provide an extensive and homogeneous sample of metallicities, potentially reaching values as low as $[\text{Fe}/\text{H}] = -4.0$. It will provide deeper CaHK imaging than most narrow-band CaHK surveys (e.g., the aforementioned Pristine and S/J-PLUS surveys) due to longer exposure times (e.g., 720s for MAGIC versus 100s for normal Pristine pointings; Starkenburg et al. 2017) and larger aperture ($\sim 4\text{m}$ for DECam versus $\sim 1\text{m}$ for S-PLUS; Mendes de Oliveira et al. 2019), allowing the identification of numerous metal-poor stars in the outer Milky Way halo, stellar streams and substructures in dwarf galaxies. The details regarding data acquisition and reduction will be presented in an upcoming early science summary paper (Chiti et al. in prep.). The initial release of the MAGIC catalog is planned for 2026. It will include fields spanning part of the Milky Way halo, in addition to observations of globular clusters, other dSphs, ultra-faint dwarf galaxies, and a portion of the outskirts of the Magellanic Clouds. We note that the data analyzed in this paper were obtained from the earliest runs of the MAGIC program (NOIRLab Prop. ID 2023B-646244; P.I. Anirudh Chiti). The field²⁰ covers about 7 half-light radii (r_h) around the center of the Scl dSph galaxy, and was obtained with three exposures of 12 minutes, dithered slightly to cover chip gaps²¹.

2.2. DELVE

DELVE (NOIRLab Prop. ID 2019A-0305; PI: Alex Drlica-Wagner), currently in its second data release (DR2²²), is a survey program that aggregates DECam data imaged by different past programs, in addition to complementing coverage with new observations (Drlica-Wagner et al. 2021, 2022). The DELVE DR2 catalogue is assembled from data collected by DELVE (Drlica-Wagner et al. 2021), Dark Energy Survey (DES; Dark Energy Survey Collaboration et al. 2016) and DECam

Legacy Surveys (DECaLS; Dey et al. 2019), besides other observing programs using the DECam, providing *griz* photometry for $\sim 17,000 \text{ deg}^2$ (around 618 million objects) with a 5σ point source depth of $g = 24.3$, $r = 23.9$, $i = 23.5$, and $z = 22.8$ mag, and a photometric accuracy of $\lesssim 20$ mmag. The mission focus is on characterizing Milky Way satellites and other stellar systems in the Local Group, as well as the discovery of new dwarf galaxies. Over the course of four years of work, numerous ultra-faint dwarf galaxies have been discovered using DELVE data (Mau et al. 2020, Cerny et al. 2021, 2023, 2024, Tan et al. 2024).

3. METHODOLOGY

The method implemented to compute photometric metallicities with the CaHK filter is similar to what was presented in Chiti et al. (2020, 2021), which we describe in this section. The notable difference is that these studies used the SkyMapper *v* filter (Keller et al. 2007) to derive metallicities, whereas here we adapt the technique to use the narrow-band CaHK filter.

3.1. Photometric metallicities

As seen in aforementioned studies, using metallicity-sensitive filters covering the CaHK region (e.g., da Costa et al. 2019, Chiti et al. 2020, Starkenburg et al. 2017, Huang et al. 2022, Placco et al. 2022, Almeida-Fernandes et al. 2023), color-color plots combining the CaHK, *g* and *i* filters can be used to distinguish different metallicities for a given surface gravity value ($\log g$). To derive metallicities in this work, we adopt the same approach as in Chiti et al. (2020, 2021), by forward-modelling fluxes through the CaHK, *g*, and *i* filters using a grid of flux-calibrated synthetic spectra spanning a range of stellar parameters. These forward-modeled fluxes are used to populate the aforementioned color-color space to map the color values to metallicities. Specifically, the grid of synthetic spectra (referred to as the TSLTE grid – TurboSpectrum with Local Thermodynamic Equilibrium) is generated using the Turbospectrum code (Alvarez & Plez 1998, Plez 2012), MARCS model atmospheres (Model Atmospheres with a Radiative and Convective Scheme; Gustafsson et al. 2008), and the line lists provided in VALD (Vienna Atomic Line Database; Piskunov et al. 1995, Ryabchikova et al. 2015).

The TSLTE grid consists of 13 values of $\log g$ equally spaced between $\log g = -0.5$ and $\log g = +5.5$, and metallicities from $[\text{Fe}/\text{H}] = -5$ to $[\text{Fe}/\text{H}] = +1$. The color-color space generated by these models in the space $\text{CaHK}_0 - g_0 + 0.9 \cdot (g - i)_0$ versus $(g - i)_0$, as shown on Figure 1, are interpolated using

²⁰ A single DECam field.

²¹ The images are publicly available in the NOIRLab Astro Archive <https://astroarchive.noirlab.edu>

²² <https://datalab.noirlab.edu/delve/>

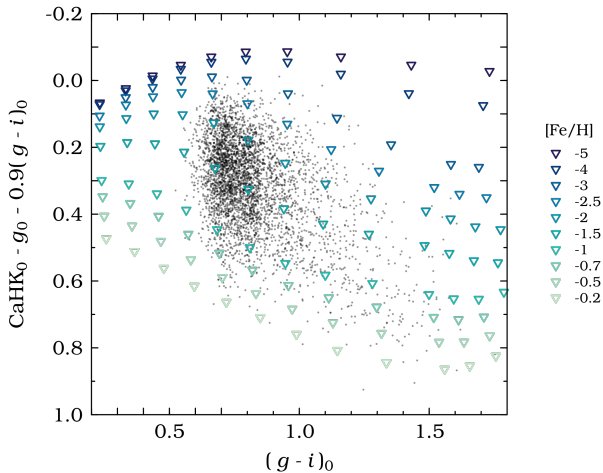


Figure 1. A color-color plot of the MAGIC data on the Scl dSph galaxy (black data points), in which the y-axis color term includes the CaHK magnitude, and the x-axis is $(g-i)_0$ color. Stars at different metallicities occupy different regions of this color-color space. To indicate this, we overplot as upside-down triangles synthetic photometry from the TSLTE grid (described in Section 3.1), fixing $\log g = 2.0$. As seen by the color-scale, stars at different metallicities separate into well-behaved trend-lines.

`scipy.interpolate.grid-data` (Virtanen et al. 2020). The subscript signifies magnitudes corrected for reddening with the Schlegel et al. (1998) dust map. For CaHK magnitudes, we adopted the extinction coefficient from Starkenburg et al. (2017): $A_{CaHK}/E(B-V) = 3.924$. The detailed process of the metallicity determination will be described in Chiti et al. (in prep.).

For each value of $\log g$, the location of the models in the color-color plot shifts slightly. Therefore, it is necessary to choose an initial $\log g$ value for the metallicity calculation. For the purpose of this work, where the distance to the stars is well-known as the distance of the Scl dSph galaxy, the initial guess of $\log g$ is derived from basic assumptions. The luminosities are estimated using the absolute magnitude of the Sun in DES g -band provided by Willmer (2018). We used the color-effective temperature transformation for giants with color $(G - G_{RP})_0$ provided by Mucciarelli et al. (2021) for Gaia DR3 photometry (Gaia Collaboration et al. 2016, Riello et al. 2021, Gaia Collaboration et al. 2023), neglecting the dependence on the metallicity, since it does not have a significant impact in the final estimates²³. Then, the stellar radii are calculated with Stefan-Boltzmann relation, and we assumed a mass of

$0.78 M_{\odot}$ for the red giant branch stars (RGB; Howell et al. 2024) to obtain the $\log g$.

The statistical uncertainty in the metallicity is derived by propagating the uncertainty in the CaHK, g , and i filters, and re-deriving the metallicity. The systematic uncertainty floor in the metallicity from this method is assumed to be 0.16 dex, following Chiti et al. (2020), who implemented the same technique and compared results to globular cluster metallicities in their study. This metallicity uncertainty floor also produces errors that are reasonably consistent with literature spectroscopic studies (see Section 4.1), indicating this is an appropriate value.

3.2. Scl dSph members

Our selection of members in the Scl dSph galaxy follows the catalog presented in Pace et al. (2022), which uses the proper motion, spatial distribution, a color-magnitude diagram selection using DECam photometry and Dartmouth isochrones (Dotter et al. 2008), and an additional color-magnitude box selection with Gaia photometry to assign a membership probability to each star. We adopted the membership probability estimated for their complete sample with a uniform background model. This sample was obtained selecting stars based on Gaia EDR3 (Gaia Collaboration et al. 2021) data: $G < 21$, renormalized unit-weight error (RUWE) < 1.4 , parallax $\varpi - 3.5\sigma_{\varpi} < 0$, and $v_{tan} - 3.5\sigma_{v_{tan}} < v_{esc}$, with the tangential (v_{tan}) and escape (v_{esc}) velocities calculated as described in Pace et al. (2022). We chose to limit the sample to stars with a membership probability greater than 0.80. We note that the selection of member stars is not particularly sensitive to the membership probability threshold that we apply, as the majority (6057 from 8768 stars in Pace et al.’s sample) have membership probabilities above 0.99.

To ensure we are analyzing the most reliable photometric metallicities, we exclude stars with final uncertainties $\sigma_{[Fe/H]} > 0.5$, which also removes those with extrapolated values in the color-color space. Only stars in the RGB region are analyzed, since the MAGIC photometric depth does not reach the turn-off region of the Scl dSph and the horizontal-branch stars are not covered by the TSLTE grid. For our isochrone selection of candidate members, we used g - and r -bands from DELVE DR2, defining an interval of 0.16 in $(g-r)_0$ color around a 12 Gyr BaSTI isochrone (Pietrinferni et al. 2004) with $[Fe/H] = -1.8$, the mean metallicity presented in Tolstoy et al. (2023). This interval was chosen to encompass most of the RGB stars, recovering members from T23. To eliminate part of the red horizontal branch within the isochrone selection, we made an additional cut, ex-

²³ Adopting an initial value of $[Fe/H] = -1.8$ would decrease the final metallicities by ~ 0.02 dex.

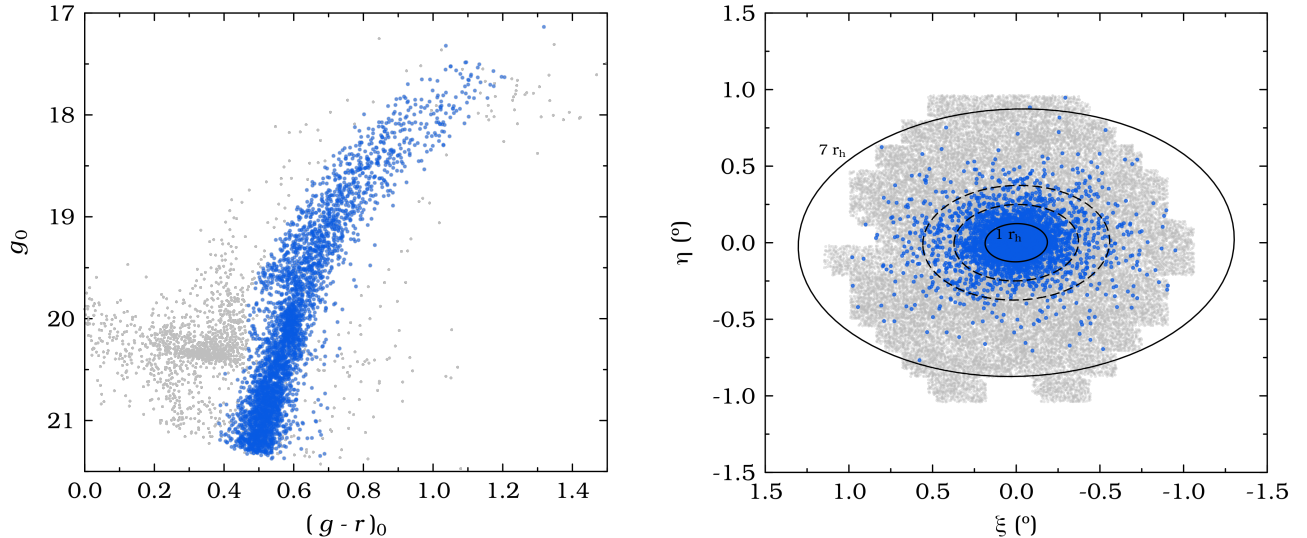


Figure 2. Left panel: color-magnitude diagram with DECam g , r photometry of selected members (blue) and the complete field observed by our DECam pointings (grey) around the Scl dSph. Right panel: Spatial distribution of selected members (blue) and the complete field (grey). The inner ellipse indicates the half-light radius for the Scl dSph galaxy ($r_h = 11.17'$). Dashed ellipses mark two and three half-light radii. The outer ellipse covers seven half-light radii, showing the extent of our data. The structural parameters used were obtained by Muñoz et al. (2018) assuming a Plummer profile.

cluding stars with $(g-r)_0 < 0.47$ and $g_0 < 20.5$. Additionally, we verified the presence of variable stars in the sample and excluded them from further analysis, by cross-matching our catalog with the Gaia DR3 variable source catalog (Gaia Collaboration et al. 2023). Likely galaxies are also removed using the `extended_class_g < 2` criterion, as described in the DELVE DR2 paper (Drlica-Wagner et al. 2022). Applying the described criteria, we found a sample of 3883 probable Scl dSph members. The left panel of Figure 2 highlights the final sample in the color-magnitude diagram.

The spatial distribution of the selected members is presented in the right panel of Figure 2, overlapped with the field observed by the DECam. Recent studies (e.g., Sestito et al. 2023) have argued that the Scl dSph stellar population may extend up to more than $\sim 9 r_h$ ($\sim 1.7^\circ$). Future MAGIC data can be used to investigate these extents in the Scl dSph. However, our current coverage ($\sim 7 r_h$; $\sim 1.3^\circ$) ought to be sufficient to capture the vast majority of the spatial extent of the Scl dSph and explore its metallicity behavior.

4. METALLICITY VALIDATION

Here, we will test the CaHK metallicities derived from the MAGIC data in the Scl dSph relative to previous spectroscopic metallicity studies. We will focus our discussion on the two largest spectroscopic samples available (de los Reyes et al. 2022, and Tolstoy et al. 2023). In the Appendix, we present a summary of the comparison with other studies available in the literature (Kirby

et al. 2009, Chiti et al. 2018, Hill et al. 2019, Reichert et al. 2020, Abdurro'uf et al. 2022, Walker et al. 2023).

4.1. Comparison to Tolstoy et al. and de los Reyes et al.

Tolstoy et al. (2023, hereafter T23) is the most extensive and homogeneous spectroscopic study of metallicities conducted so far for the Scl dSph galaxy, in which metallicities for more than a thousand confirmed members were derived from the Ca II triplet lines from the VLT Fibre Large Array Multi-Element Spectrograph (FLAMES) low-resolution data. Given the size and quality of this sample, we will use their estimates to verify the reliability of MAGIC metallicities. Following the suggested quality flags described in that paper, only members in their study with signal-to-noise ratio > 13 and no flag indicating sky subtraction residuals were selected. This gives a sample of 1148 stars observed and measured by MAGIC in common with T23.

The other spectroscopic study we compare to, de los Reyes et al. (2022, hereafter R22), compiled data from previous works obtained with the Deep Imaging Multi-Object Spectrometer (DEIMOS) on the Keck II telescope (Faber et al. 2003) and by the Dwarf Abundances and Radial Velocities Team (DART; Tolstoy et al. 2006). Metallicities and α -abundances were derived using spectral synthesis by Kirby et al. (2010), being both an independent dataset and method compared to the T23 analysis. From the 465 stars in their sample, we found

366 in common with the MAGIC survey, located mainly in the central region of the Scl dSph galaxy.

The upper panels in Figure 3 show the comparison between the MAGIC-derived photometric metallicities presented in this work and the spectroscopic values reported by R22 and T23. The lower panels present the difference between the MAGIC estimates and the spectroscopic data, with which the median offsets were calculated. Both estimates exhibit an overall good agreement with the $[\text{Fe}/\text{H}]_{\text{MAGIC}}$, with no notable trend compared to the larger T23 sample.

For $[\text{Fe}/\text{H}]_{\text{MAGIC}} < -2.5$, we do not have a good sampling in R22, since it mainly covers the central region of Scl dSph. In the same interval, we note that the 70 stars in common with T23 tend to be more metal-poor in the MAGIC data, being ~ 0.17 dex lower than the reported spectroscopy. Stars with $[\text{Fe}/\text{H}]_{\text{MAGIC}} > -1$ in both panels tend to be ~ 0.36 dex overestimated and exhibit a larger scatter. Between $[\text{Fe}/\text{H}]_{\text{MAGIC}} = -2.5$ and $[\text{Fe}/\text{H}]_{\text{MAGIC}} = -1$, the photometric values are in excellent agreement with the spectroscopic ones. The median offset observed in this interval for R22 is 0.08 dex and for T23 is -0.02 dex, with median absolute deviations of 0.22 dex in each case. The overall median offset for R22 is 0.09 dex. For T23, we find -0.02 dex. Except for the caveats mentioned, these comparisons make us confident that MAGIC photometric $[\text{Fe}/\text{H}]$ values are robust and can be used to study stellar populations properties of this dwarf galaxy, for the bulk of its metallicity range. We note that the MAGIC metallicity calibration is based only on the synthetic isochrones and has not been tuned to the spectroscopic data.

The metallicity uncertainties ($\sigma_{[\text{Fe}/\text{H}]}$) for all members of the Scl dSph observed by MAGIC, as well as for the stars in common between MAGIC and spectroscopic works, as a function of g_0 magnitude are presented in the upper panel of Figure 4. Note that our uncertainties are usually larger than the values reported in R22 and T23 due to the systematic uncertainty floor adopted. For stars with $g_0 \sim 20$, our uncertainties are comparable to those reported by T23. Nearly all stars with $g_0 < 20$ have associated $\sigma_{[\text{Fe}/\text{H}]}$ smaller than 0.3 dex, and approximately 86% of the entire sample fall within this uncertainty threshold.

The bottom panel in Figure 4 presents the normalized difference histogram, i.e.,

$$\frac{[\text{Fe}/\text{H}]_{\text{MAGIC}} - [\text{Fe}/\text{H}]_{\text{spec}} - C}{\sqrt{\sigma_{\text{spec}}^2 + \sigma_{\text{MAGIC}}^2}}, \quad (1)$$

where C is the overall median offset between MAGIC metallicity estimates and the spectroscopic works, and

σ are the respective metallicity uncertainties. The yellow line corresponds to the comparison with R22's work, and the green line, to T23's work. Means, medians, standard deviations and median absolute deviations for both distributions are presented in Table 1. As previously note in Figure 3, there is a good agreement between MAGIC photometric metallicities and the spectroscopic estimates, with standard deviations of both distributions close to 1. The gray curve represents a Gaussian curve with mean $\mu = 0$ and standard deviation $\text{SD} = 1$, serving as a reference to highlight the agreement between the estimates.

Stars with photometry that has been de-blended in either the CaHK, g -, or i -band data receive a flag in our catalogue (`feh_flag_phot`). Nearly 44% of the selected members in the Scl dSph, mainly those in the inner region, are flagged. However, we observed that it does not seem to significantly affect the estimated metallicity. Figure 5 presents the comparison with T23 considering possible blending issues with the photometry. Stars without photometric flags are shown in the blue (upper panel), while stars with photometric flags are plotted as grey points (lower panel). When comparing with T23 data, we found 484 members with possible problematic observations. However, it does not seem to have a high impact in our metallicity estimates, since both subsets present a small offset (0.02 and -0.04 , with and without the flags, respectively). We do note that most stars with $[\text{Fe}/\text{H}]_{\text{MAGIC}} > -1$ may be affected.

4.2. Photometric metallicities for carbon-enhanced metal-poor stars

It is important to verify the photometric metallicity estimates for carbon enhanced metal-poor (CEMP) stars (Beers & Christlieb 2005), since high carbon-abundances increase the strength of the CN feature blueward of the Ca II K line, suppressing the flux in the CaHK filter and making the star appear more metal-rich (Chiti et al. 2020, Martin et al. 2024). Therefore, an additional analysis was performed considering the Chiti et al. (2018) sample, which obtained medium-resolution spectra with the Michigan/Magellan Fiber System on the Magellan-Clay telescope for 100 stars in the Scl dSph. They estimated $[\text{Fe}/\text{H}]$, from the Ca II K line, and $[\text{C}/\text{Fe}]$ from the CH G-band at $\sim 4300\text{\AA}$. Here, we found 64 members in common, with which we can compare the photometric estimates and observe the influence of the carbon abundance on the photometric metallicity determination.

Figure 6 shows the difference between $[\text{Fe}/\text{H}]_{\text{MAGIC}}$ and $[\text{Fe}/\text{H}]_{\text{C18}}$, colored by the carbon abundance reported in their work, where the carbon abundances are

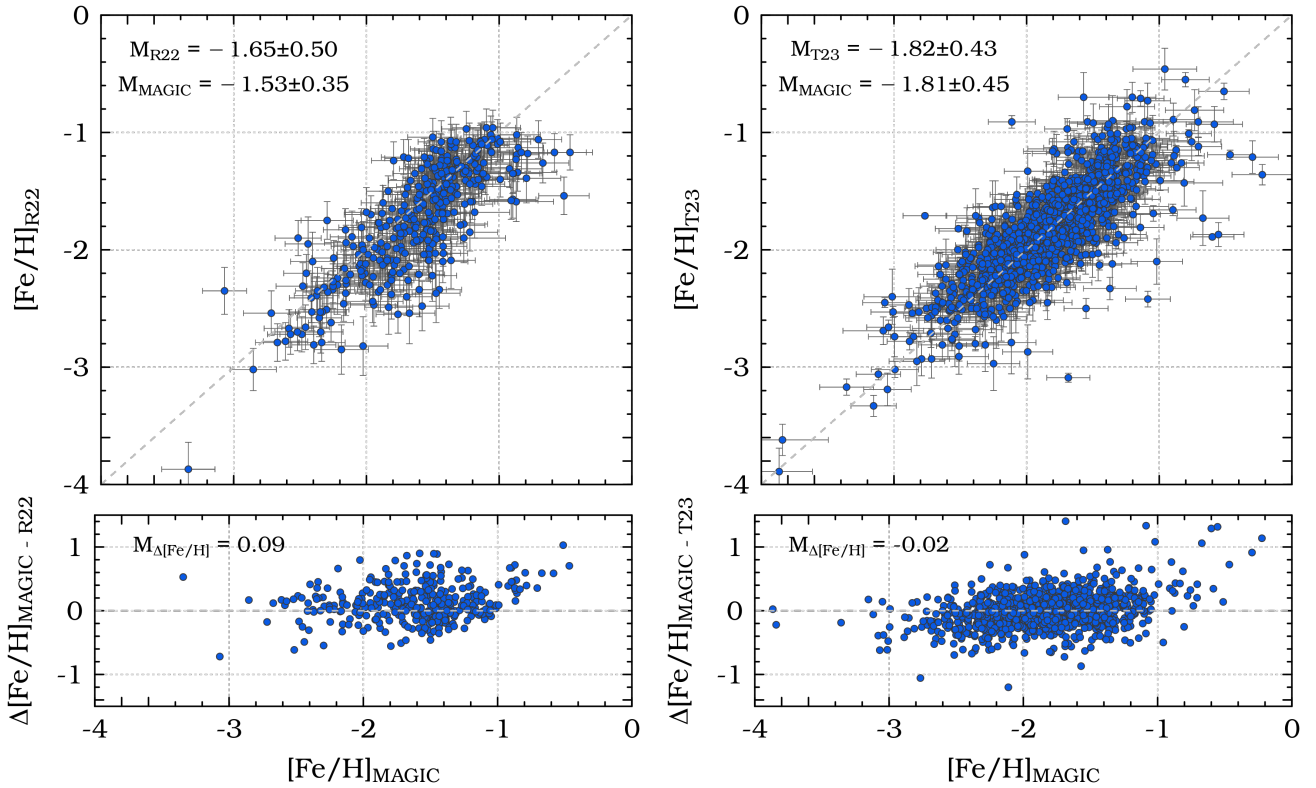


Figure 3. Top panels: comparison between the derived photometric metallicity values in this work and in spectroscopic work in the literature by de los Reyes et al. (2022) (left) and Tolstoy et al. (2023) (right). Median values and median absolute deviations (M_{MAGIC} , M_{R22} , and M_{T23}) are indicated in the top left corner of each panel. Bottom panels: difference between the $[\text{Fe}/\text{H}]_{\text{MAGIC}}$ and the spectroscopic estimates. $M_{\Delta[\text{Fe}/\text{H}]}$ indicates the median value.

not corrected for the evolutionary state of the star. Stars with uncorrected $[\text{C}/\text{Fe}]_{\text{C18}} < -0.5$ exhibit a reasonable scatter between the estimates, with a median offset of 0.24 dex. On the other hand, stars with a higher $[\text{C}/\text{Fe}]_{\text{C18}}$ tend to have higher values of $[\text{Fe}/\text{H}]_{\text{MAGIC}}$ compared to $[\text{Fe}/\text{H}]_{\text{C18}}$. This may be due to the absorption of the CN band found at the edge of bluer wavelengths of the filter. In Figure 6, we observe that higher carbon abundances can cause higher photometric metallicities, with a median overestimation of ~ 0.38 dex. This effect is also noted in, e.g., Martin et al. (2024), and may possibly explain the overestimation of $[\text{Fe}/\text{H}]$ observed in Figure 3 for stars with $[\text{Fe}/\text{H}]_{\text{MAGIC}} > -1$. There seems to be a slight trend with $[\text{C}/\text{Fe}]_{\text{C18}}$, where metallicities for stars with carbon abundance higher than $[\text{C}/\text{Fe}]_{\text{C18}} \approx -0.5$ are progressively overestimated for higher $[\text{Fe}/\text{H}]_{\text{MAGIC}}$, while stars with lower values do not show the same trend. However, this interpretation is limited due to the small number of stars in the comparison that have $[\text{Fe}/\text{H}]_{\text{MAGIC}} > -2$ to affirm that it is the cause of the metallicity overestimation.

Nevertheless, we do not expect this systematic to meaningfully affect the analysis presented in this paper. From the observed bias, we can calculate that,

considering that 11%²⁴ of the Scl dSph members with $[\text{Fe}/\text{H}]_{\text{MAGIC}} > -2$ are stars with $[\text{C}/\text{Fe}]_{\text{C18}} > -0.5$, the median metallicity would be overestimated by ~ 0.10 dex. We therefore do not expect the results to follow to be strongly affected by the carbon abundances. More generally, evidence that this systematic ought not to affect our interpretation also follows from the comparisons in Figure 3. The MAGIC photometric metallicities show good agreement with spectroscopic metallicities across large numbers of stars in the Scl dSph that were not pre-selected based on carbon, likely spanning the characteristic range of $[\text{C}/\text{Fe}]$ for the galaxy.

5. RESULTS & DISCUSSION

After verifying the performance of the photometric metallicities, we can inspect the characteristics of the Scl dSph. The new sample offers a significant advantage over spectroscopy, as it is both spatially unbiased and represents the largest dataset of metallicities in the lit-

²⁴ This value was adopted based on the number of stars in Chiti et al. (2018) with $[\text{C}/\text{Fe}]_{\text{C18}} > -0.5$ and $[\text{Fe}/\text{H}]_{\text{MAGIC}} > -2$, which corresponds to the metallicity range where most of our sample is found.

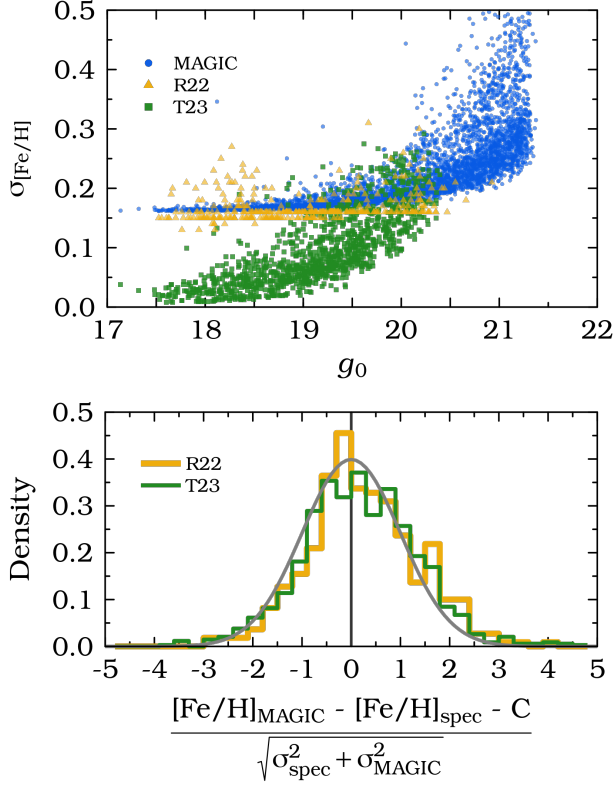


Figure 4. Top panel: metallicity uncertainties as a function of g_0 magnitude for members observed by the MAGIC survey (blue points), and stars in common with [de los Reyes et al. \(2022; R22](#) – yellow triangles) and with [Tolstoy et al. \(2023; T23](#) – green squares). Bottom panel: normalized difference histograms comparing MAGIC estimates with [R22](#) (yellow thick line) and [T23](#) (green thin line). The gray curve illustrates a Gaussian function with mean = 0 and standard deviation = 1 for comparison.

erature to date (~ 3800 stars) in any dSph galaxy. This is the first application of the MAGIC data, showing how our photometric metallicities can help construct a more complete spatial view of systems as distant as the Milky Way satellites.

5.1. Metallicity distribution

Panel (a) of [Figure 7](#) presents the cumulative distribution function of the projected distance measure in r_h of the stars in the Scl dSph observed by [R22](#), [T23](#), and this study, indicating the spatial distribution of the members. The data used in [R22](#) (yellow thick line) are more restricted to the core, which is the more metal-rich part of the galaxy. Panel (b) of [Figure 7](#) shows the different MDFs for each work. The [R22](#) MDF peaks at higher values, with a median of $[\text{Fe}/\text{H}]_{\text{R22}} = -1.62$, and exhibits an extended metal-poor tail. On the other hand, [T23](#) (green thin line) covered a larger area and observed more

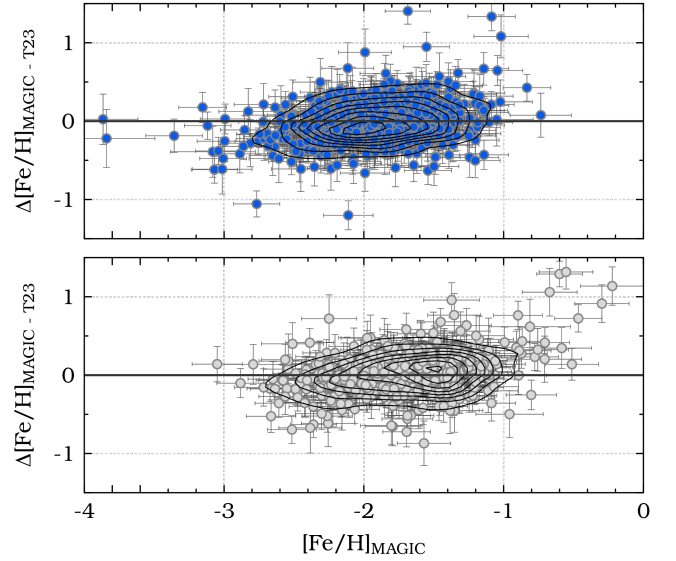


Figure 5. Comparison of photometric metallicities and spectroscopic metallicities from [T23](#) separating the sample between stars with (bottom panel) and without (top panel) de-blended photometry. Contours were added to highlight the density distribution of the data points.

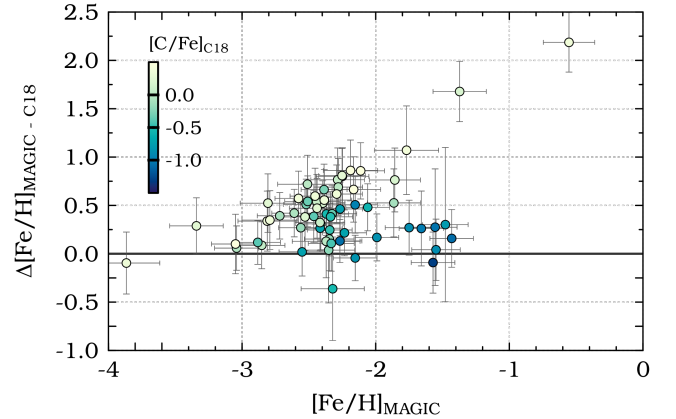


Figure 6. Difference between photometric metallicity and spectroscopic values, colored according to the measured carbon abundance for each star. Both spectroscopic $[\text{Fe}/\text{H}]$ and $[\text{C}/\text{Fe}]$ are reported by [Chiti et al. \(2018\)](#).

metal-poor stars toward the outskirts of the galaxy, resulting in a median $[\text{Fe}/\text{H}]_{\text{T23}} = -1.83$. The spatial coverage obtained in this work spans the inner and outer regions of the galaxy, since there is no prior target selection for our observations, as required for spectroscopy. Therefore, our data displays an MDF with a peak more metal-rich than [T23](#), more consistent with [R22](#). The main statistical parameters for the MDF with MAGIC estimates are presented in [Table 1](#). The median metallic-

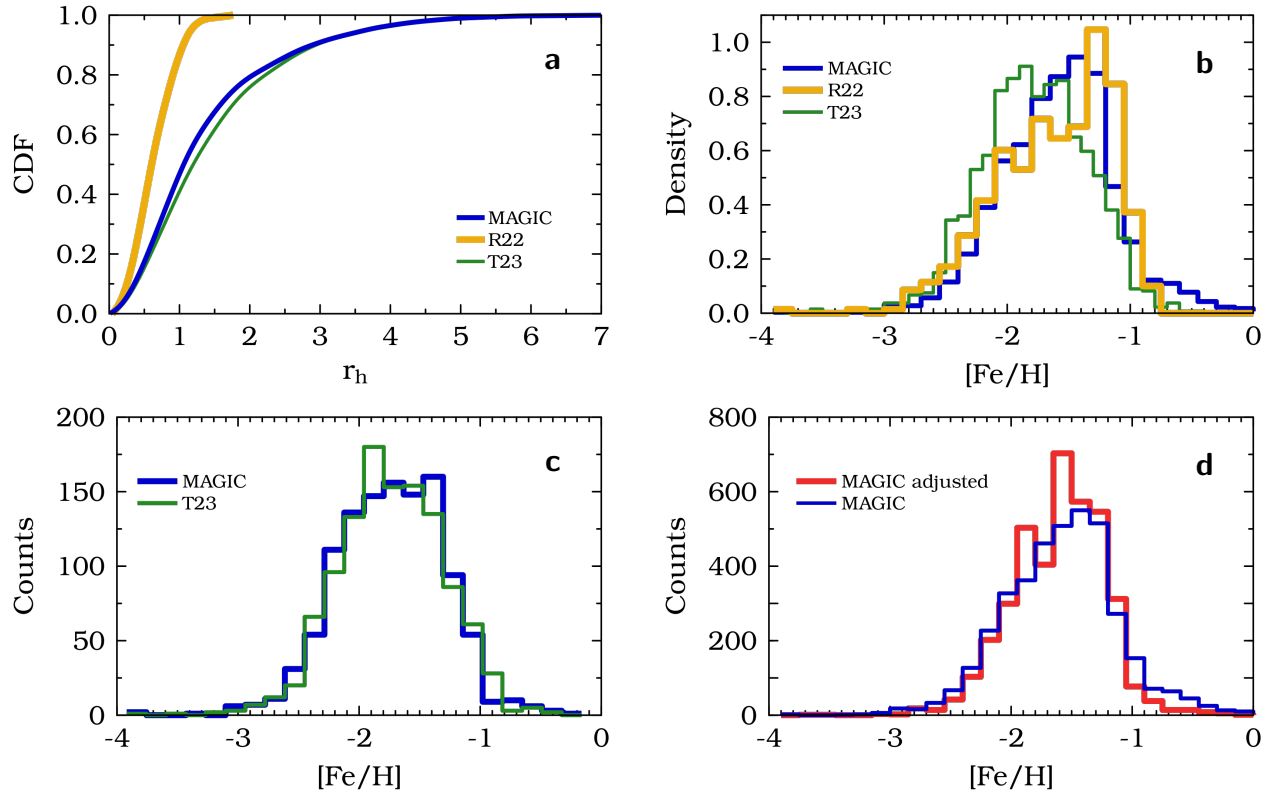


Figure 7. Panel (a): cumulative distribution function as a function of half-light radius. The blue line indicates the data obtained with MAGIC observations; the yellow thick line, with [de los Reyes et al. \(2022; R22\)](#); the green thin line, with [Tolstoy et al. \(2023; T23\)](#). Panel (b): comparison of the MDF for the different studies of the Scl dSph galaxy. Panel (c): comparison between photometric (MAGIC) and spectroscopic (T23) data for members in common. Panel (d): MDFs for estimated (thin blue line) and adjusted (thick red line) MAGIC metallicities.

ity obtained is $[\text{Fe}/\text{H}]_{\text{MAGIC}} = -1.63$ and a Kolmogorov-Smirnov test reinforces that the MAGIC MDF is statistically different from T23 spectroscopic sample, with a p-value < 0.001 , while comparing with R22 sample we find p-value ~ 0.13 .

Panel (c) of Figure 7 shows the MDFs of MAGIC photometric estimates (blue line) and the spectroscopic ones from T23 (green line), when considering only the members in common between the samples. Both MDFs appear similar, with a MAGIC median value of $[\text{Fe}/\text{H}]_{\text{MAGIC}} = -1.81$ in excellent agreement with T23 measurements. This result suggests that the discrepancy observed in the MDFs of the entire MAGIC and T23 samples presented in the top panel of Figure 7 is likely due to spatial sampling.

Panel (d) of Figure 7 presents the MDF obtained for MAGIC metallicities adjusted to align with T23 estimates, using the median offset between $[\text{Fe}/\text{H}]_{\text{MAGIC}}$ and $[\text{Fe}/\text{H}]_{\text{T23}}$ in bins of 0.2 dex. Bins with less than five stars receive the offset calculated in the closest bin. This adjustment principally accounts for some system-

atics that we discuss in Section 4.1, where stars with $[\text{Fe}/\text{H}]_{\text{MAGIC}} > -1.0$ have overestimated metallicities and those with $[\text{Fe}/\text{H}]_{\text{MAGIC}} < -2.5$ are slightly underestimated. We emphasize that this procedure is intended to bring MAGIC metallicities to the same scale as T23, allowing us to isolate the impact of spatial bias. However, it does not represent our final adopted metallicity estimates. After this adjustment, we still find a more metal-rich peak, with a median value of $[\text{Fe}/\text{H}]_{\text{adjusted}} = -1.63$ and a median absolute deviation of 0.39 dex.

Our method performs well on the lower metallicity regime, potentially estimating metallicities below $[\text{Fe}/\text{H}] = -3.5$. We find 132 members with $[\text{Fe}/\text{H}]_{\text{MAGIC}} < -2.5$, nearly doubling the number of stars in this regime when compared to T23 (74 stars). Furthermore, going to even lower metallicities, we can identify 20 EMP stars. Among the stars in common with MAGIC observations, T23 found 12 EMP stars, and seven of them are also identified as EMP by MAGIC metallicity (one being flagged as potential blend). Five

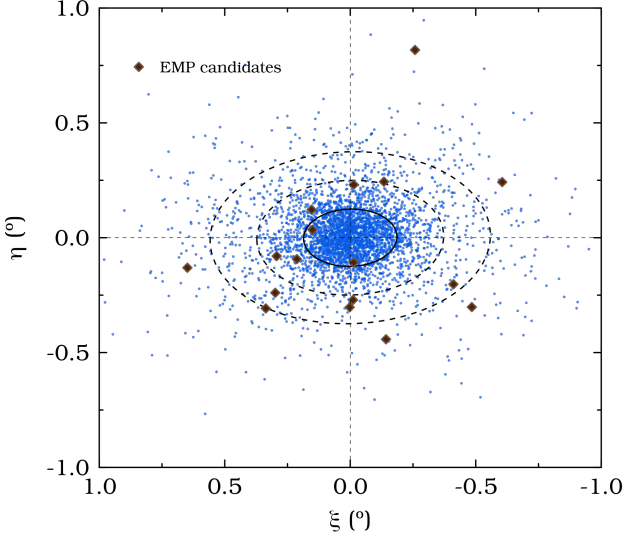


Figure 8. Spatial distribution of Scl dSph members (small dots) and EMP candidates ($[\text{Fe}/\text{H}]_{\text{MAGIC}} < -3.0$; diamonds) from our MAGIC photometric metallicity data.

other stars would be classified as possible EMP stars by MAGIC metallicities, however they appear to be more metal-rich by T23, with $-2.7 \leq [\text{Fe}/\text{H}]_{\text{T23}} \leq -2.4$. This represents a success rate of $\sim 58\%$ for the detection of EMP stars in our sample. Notably, we also find six stars in the Scl dSph with $[\text{Fe}/\text{H}]_{\text{MAGIC}} < -3$ with no counterpart in the literature. However, these stars are faint ($G > 19$), making them feasible targets for the next generation of spectroscopic surveys.

Recently, Arroyo-Polonio et al. (2024) suggested the existence of a third chemodynamical stellar population in the Scl dSph galaxy, characterized by a higher mean line-of-sight velocity, a very low metallicity ($[\text{Fe}/\text{H}] < -2$), and a distinctly asymmetric spatial distribution. Here, we recover this peculiar behaviour in the sky projection of the MAGIC EMP candidates. In Figure 8, we highlight 17 EMP stars identified and note that most of them (11) are preferentially found on the southern region of the galaxy. Three EMP candidates were removed as they possess velocities measured by T23 below 110 km s^{-1} and certainly do not compose this group according to Arroyo-Polonio et al. (2024)’s classification. Further radial velocity analysis is required to confirm whether these candidates, as well as new very metal-poor stars observed by MAGIC, are members of this newly discovered Scl dSph population.

5.2. Metallicity gradient

Numerous works have demonstrated that dwarf galaxies usually cannot be modeled by a single stellar component (e.g., Ural et al. 2010, de Boer et al. 2012, Pace

Table 1. Summary of statistics for the MAGIC MDF (Figure 7), including mean, median, standard deviation (SD), median absolute deviation (MAD), skewness, kurtosis, and quantiles (25th and 75th). Mean and median values with their respective deviation for the normalized difference (ND) histograms (Figure 4) are listed here. The metallicity gradients estimated by single and segmented fits (SF) are also presented.

| MAGIC MDF | |
|---------------------------|--|
| Median \pm MAD | -1.63 ± 0.42 |
| Mean \pm SD | -1.66 ± 0.47 |
| Skewness | 0.03 |
| Kurtosis | 3.87 |
| 25th / 75th quantiles | $-1.96 / -1.37$ |
| ND: Tolstoy et al. - | $\frac{[\text{Fe}/\text{H}]_{\text{MAGIC}} - [\text{Fe}/\text{H}]_{\text{T23-C}}}{\sqrt{\sigma_{\text{T23}}^2 + \sigma_{\text{MAGIC}}^2}}$ |
| Median \pm MAD | 0.0 ± 1.1 |
| Mean \pm SD | 0.0 ± 1.3 |
| ND: de los Reyes et al. - | $\frac{[\text{Fe}/\text{H}]_{\text{MAGIC}} - [\text{Fe}/\text{H}]_{\text{R22-C}}}{\sqrt{\sigma_{\text{R22}}^2 + \sigma_{\text{MAGIC}}^2}}$ |
| Median \pm MAD | 0.0 ± 1.0 |
| Mean \pm SD | 0.1 ± 1.1 |
| Metallicity gradients | |
| Single linear fit | $-1.03 \pm 0.03 \text{ dex deg}^{-1}$ $-0.19 \pm 0.01 \text{ dex } r_h^{-1}$ $-0.70 \pm 0.18 \text{ dex kpc}^{-1}$ |
| SF: until $1.06 r_h$ | $-3.35 \pm 0.18 \text{ dex deg}^{-1}$ $-0.62 \pm 0.03 \text{ dex } r_h^{-1}$ $-2.29 \pm 0.60 \text{ dex kpc}^{-1}$ |
| SF: beyond $1.06 r_h$ | $-0.56 \pm 0.26 \text{ dex deg}^{-1}$ $-0.10 \pm 0.05 \text{ dex } r_h^{-1}$ $-0.38 \pm 0.20 \text{ dex kpc}^{-1}$ |

et al. 2020), and the Scl dSph is not an exception. Observing horizontal-branch stars, Tolstoy et al. (2004) revealed that most of the redder (more metal-rich and younger) stars tend to be found in the inner region, whereas the blue ones (more metal-poor and older) are found in the outskirts. Since then, the metallicity gradient of the Scl dSph has been quantified with more robust samples (Kirby et al. 2009, 2011, Leaman et al. 2013, Ho et al. 2015, Martínez-Vázquez et al. 2016, Taibi et al. 2022, Tolstoy et al. 2023).

Here, we quantify the metallicity gradient of the Scl dSph with MAGIC data. Figure 9 presents the cumulative distribution function in units of r_h , which reflects the metallicity gradient of the galaxy. We adopted $r_h = 11.17'$, as provided by Muñoz et al. (2018). The metallicity intervals shown contain 20, 859, 1542, 1202, 260 stars from $[\text{Fe}/\text{H}]_{\text{MAGIC}} < -3$ to $[\text{Fe}/\text{H}]_{\text{MAGIC}} > -1$,

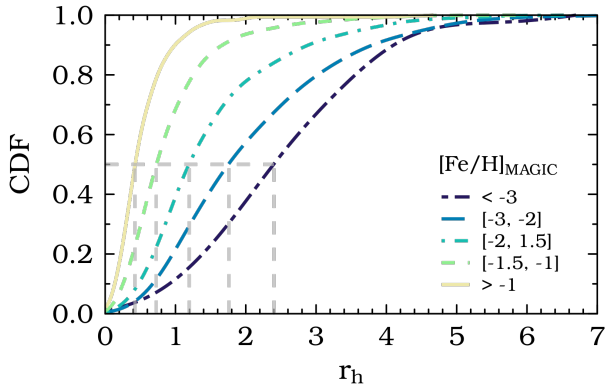


Figure 9. Cumulative distribution functions for the Scl dSph members at different metallicity intervals.

respectively. The distributions show that stars more metal-rich are found mainly in the inner regions, while more metal-poor stars populate from the center to the outermost part of the galaxy. Beyond $\sim 3 r_h$, we find few stars with $[\text{Fe}/\text{H}]_{\text{MAGIC}} > -1.5$. The dashed gray lines indicate 2.4, 1.8, 1.2, 0.7, and 0.4 r_h , which correspond to the radii enclosing approximately 50% of the stars in each subsample.

Figure 10 shows the variation of metallicity with r_h with MAGIC data (top panel) and a comparison of the metallicity gradients reported in the literature (bottom panel). The black line illustrates a piecewise linear fit to the MAGIC metallicities obtained using the `segmented R` package (Muggeo 2003). It evidences a sharp decrease in metallicity until $1.06 \pm 0.04 r_h$ ($\sim 11.8'$), followed by an almost constant trend. The first slope measures a gradient of $-3.35 \pm 0.18 \text{ dex deg}^{-1}$ and, after the break point, we find a shallower slope of $-0.56 \pm 0.26 \text{ dex deg}^{-1}$. The red line indicates the segmented fit obtained for MAGIC metallicities adjusted to the T23 metallicity scale by the median offsets for bins of 0.2 dex (see discussion in Section 5.1). It slightly changes to $-2.54 \pm 0.15 \text{ dex deg}^{-1}$ and $-0.48 \pm 0.21 \text{ dex deg}^{-1}$, with a break-point at $1.07 \pm 0.05 r_h$.

A double fit, with a stronger inner gradient, is also detectable in spectroscopic data. When applying the segmented fit to T23 data, we find an inner gradient of $-1.51 \pm 0.24 \text{ dex deg}^{-1}$ and a flatter gradient beyond $1.35 \pm 0.19 r_h$, with a value of $-0.38 \pm 0.36 \text{ dex deg}^{-1}$. This result reiterates that the inner region of the Scl dSph is more chemically enriched compared to the outer region (e.g., Martínez-Vázquez et al. 2016, Bettinelli et al. 2019). The outer gradients obtained with both MAGIC and T23 are both weaker compared with previous estimates in the literature ($-1.44 \text{ dex deg}^{-1}$; Leaman et al. 2013, and $-1.50 \text{ dex deg}^{-1}$ for RR Lyrae stars beyond $32'$; Martínez-Vázquez et al. 2016).

A single linear fit to MAGIC metallicities results in a gradient of $-1.03 \pm 0.03 \text{ dex deg}^{-1}$ ($-0.70 \pm 0.18 \text{ dex kpc}^{-1}$). The trend is expected to be stronger with our estimates compared to T23, as our sample comprises more stars in the center of the galaxy. The metallicity gradient presented by T23, of $-0.70 \text{ dex deg}^{-1}$, agrees very well with the estimation from Taibi et al. (2022) ($-0.68 \pm 0.05 \text{ dex deg}^{-1}$). Our gradient highly exceeds those measurements and might be inflated by the metallicity overestimation observed for $[\text{Fe}/\text{H}]_{\text{MAGIC}} > -1$. Nevertheless, when only stars without photometric flags (i.e., from de-blending) are considered, our data still implies a stronger metallicity gradient of $-0.79 \pm 0.04 \text{ dex deg}^{-1}$ likely due to our unbiased spatial sampling. If the MAGIC metallicities are adjusted to the T23 metallicity scale by the median offsets in bins of 0.2 dex, the linear gradient decreases to $-0.86 \pm 0.03 \text{ dex deg}^{-1}$ ($-0.58 \pm 0.15 \text{ dex kpc}^{-1}$). This value also indicates a stronger metallicity gradient than the fit obtain with T23 data, reinforcing that this is a result of our sample being spatially unbiased.

The origin of metallicity gradients is still unclear. It could be a consequence of secular evolution, with more metal-rich stars being formed at the central region, where the potential is stronger and gas density is higher (Kennicutt 1983, Schroyen et al. 2013, Revaz & Jablonka 2018). Another possibility is that, with successive rounds of star formation over time, earlier generations of stars are pushed to the outskirts by supernova feedback (El-Badry et al. 2016, Mercado et al. 2021). Moreover, accretion events may impact the metallicity gradient, either strengthening or diminishing it (e.g., Benítez-Llambay et al. 2016, Cardona-Barrero et al. 2021, Taibi et al. 2022). Just recently, observations of metallicity variations along the stream of the Sagittarius dSph (e.g., Majewski et al. 2003) have been linked to a rapid formation of a metallicity gradient in this galaxy, which should have been in place already at redshift $z \sim 0.5$ (Limberg et al. 2023, Cunningham et al. 2024).

Strong metallicity gradients were previously reported for the Scl dSph (e.g., $-1.86 \text{ dex deg}^{-1}$ by Kirby et al. 2011 and $-1.57 \text{ dex deg}^{-1}$ by Ho et al. 2015) and are indeed expected for systems with distinct chemodynamical populations. Benítez-Llambay et al. (2016) discussed the possible role of mergers in the formation of the Scl dSph, being responsible for the spatial segregation of the metal-rich and metal-poor populations. Minor mergers might contribute to the less pronounced gradients in the outer region of the galaxy. Arroyo-Polonio et al. (2024) argue that the asymmetry in the spatial distribution could be the result of a recent merger event in the Scl dSph. In this study, the smooth decline be-

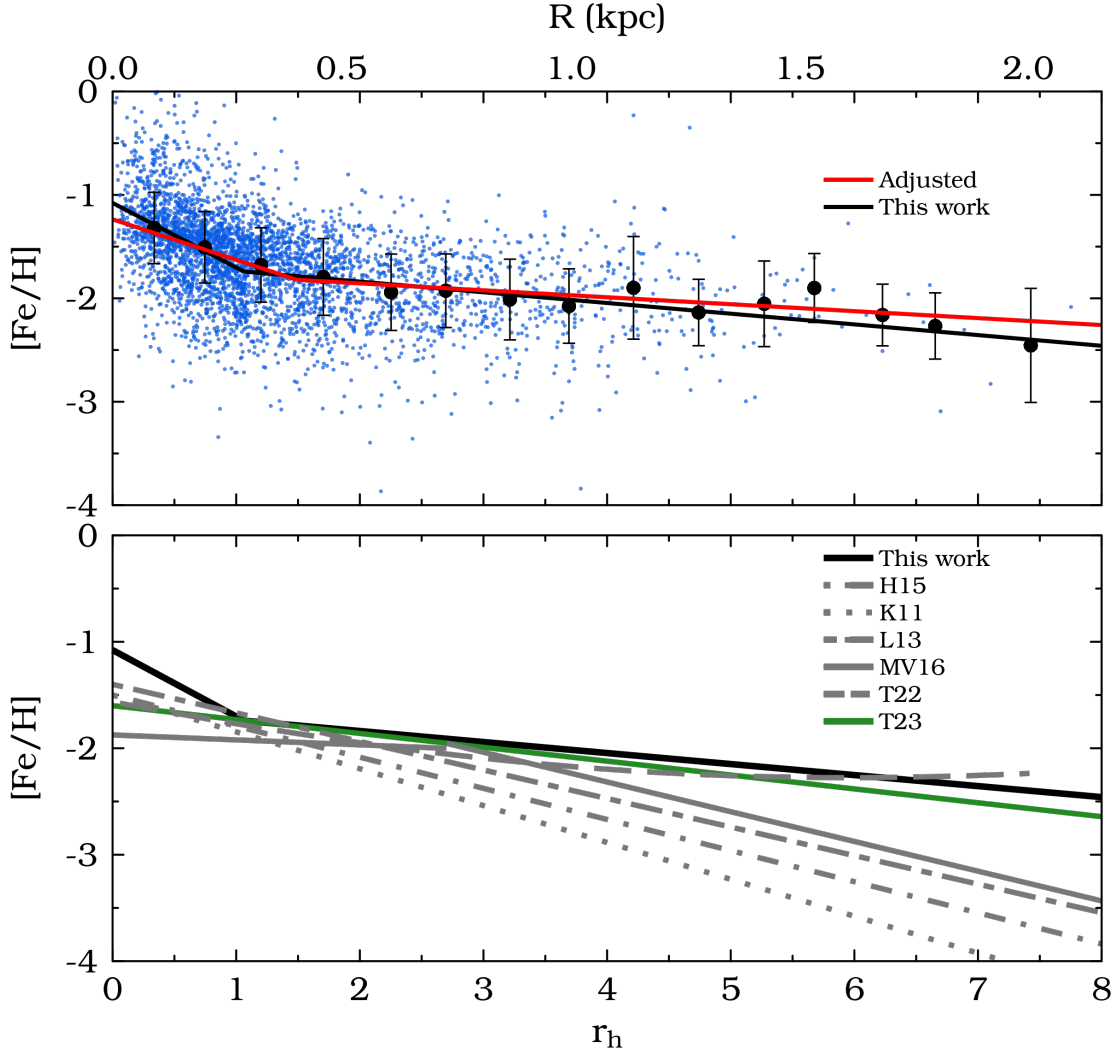


Figure 10. Top panel: metallicities of the Scl dSph members as a function of half-light radius/projected distance. Black points represent median $[\text{Fe}/\text{H}]_{\text{MAGIC}}$ values in bins of $0.5 r_h$. The black line represents a piecewise fit (inner fit: slope = -0.62 and intercept = -1.08 ; outer fit: slope = -0.10 and intercept = -1.63). The red line shows the segmented fit performed for adjusted MAGIC metallicities, brought to T23 scale. Bottom panel: metallicity gradients obtained in this work, along with previous estimates reported in the literature. We present metallicity gradients from Kirby et al. (2011; K11), Leaman et al. (2013; L13), Ho et al. (2015; H15), Martínez-Vázquez et al. (2016; MV16), Taibi et al. (2022; T22), and Tolstoy et al. (2023; T23).

yond $1.06 r_h$ suggests a weak gradient in the outskirts, however, it is not definitive evidence for a merger. If this gradient is a real feature, it may potentially also hint at the hierarchical formation occurring in this galaxy.

6. CONCLUSIONS & SUMMARY

This work presents a comprehensive study of the photometric metallicities of stars in the Scl dSph galaxy from the DECam MAGIC survey, including 3883 member stars out to seven times its half-light radius. Our study roughly triples the numbers of stars in the literature with spectroscopic metallicities, and allows us to derive the metallicity properties of the system in a

spatially unbiased manner into the far outskirts of the system. Given the Scl dSph’s status as a “textbook” dwarf galaxy that is well-studied, we use the extensive literature data to validate our photometric metallicity estimates and to assess the utility of our program on other dwarf galaxies in the near future.

We find that the metallicity derived from the CaHK filter agrees well with spectroscopic data, especially between $-2.5 < [\text{Fe}/\text{H}]_{\text{MAGIC}} < -1$, with a median offset around -0.02 dex. For stars more metal-rich than -1 , MAGIC metallicities tend to be higher, with an offset of ~ 0.35 dex, while the opposite is observed for

stars with $[\text{Fe}/\text{H}]_{\text{MAGIC}} < -2.5$ (offset ~ -0.19 dex). When comparing only stars in common, our estimates recover an MDF very similar to the one obtained by Ca II triplet metallicities in the T23 study of ~ 1400 stars, with a median value of $[\text{Fe}/\text{H}]_{\text{MAGIC}} = -1.81$ and a median absolute deviation of 0.45 dex. The agreement with spectroscopic values demonstrates the reliability of our measurements.

Our study shows that the MDF of the Scl dSph galaxy exhibits a characteristic expected for dSph systems: a sharp metal-rich end, an indication of star formation interrupted in dSph satellites by ram pressure stripping (Kirby et al. 2013, Ross et al. 2015). The radial distribution shows a clear change in the spatial distribution of stars according to their metallicities, with the radii enclosing approximately 50% of the stars increasing from $0.4 r_h$ to $2.4 r_h$ for those with $[\text{Fe}/\text{H}]_{\text{MAGIC}} > -1$ and $[\text{Fe}/\text{H}]_{\text{MAGIC}} < -3$, respectively. We estimated a metallicity gradient of $-3.35 \pm 0.18 \text{ dex deg}^{-1}$ for stars inside $1.06 r_h$ and $-0.56 \pm 0.26 \text{ dex deg}^{-1}$ for the outer part of the galaxy. The internal metallicity gradient is stronger than previously estimated, incompatible with values reported by recent spectroscopic works (Taibi et al. 2022 and Tolstoy et al. 2023), which is likely due to the lack of more metal-rich stars found in the center of the Scl dSph in previous samples. However, it is important to clarify that this value is affected by the apparently worse performance noticed for $[\text{Fe}/\text{H}]_{\text{MAGIC}} > -1$ in the MAGIC photometric metallicity estimates, even though we still expect a stronger gradient when stars in central regions are accessed.

The MAGIC photometric metallicities exhibit promising performance, even into the lowest metallicity regimes, as observed in the bottom panel of Figure 7. This allows us to further investigate the low metallicity population in our sample. Comparing with T23 spectroscopic data, we obtain a success rate of $\sim 58\%$ in identifying stars below $[\text{Fe}/\text{H}] = -3$. Furthermore, we found six EMP candidates without spectroscopic confirmation in the literature. All the stars present magnitudes $G > 19$, which makes it difficult to perform spectroscopic follow-up using facilities currently in operation. Still, it is another example of how investigating photometric metallicities can be useful in distant galaxies. Additional studies in the outer region in the Scl dSph and other dwarf galaxies are essential to find the most metal-poor stars in these systems.

This paper provides a demonstration of the power of the photometric metallicity technique with the CaHK narrow-band filter used by the MAGIC survey, building on the success of photometric metallicity studies of dwarf galaxies in the past (e.g., Chiti et al. 2020, 2021,

Vitali et al. 2022, Longeard et al. 2022, Fu et al. 2023, 2024b, Pan et al. 2025). Notably, we can obtain much larger samples of members for dwarf galaxies without target-selection biases introduced by spectroscopic studies. In the future, we will expand this analysis to other Local Group dSph galaxies less well-studied than the Scl dSph, providing important population-level constraints regarding their evolution through the properties of their stellar populations (e.g., MDFs, spatial-metallicity correlations). The MAGIC survey is still ongoing, with an upcoming early science paper (Chiti et al. in prep.), and additional work relevant to dwarf galaxies including an exploration of members in the outskirts of classical dSphs (Pace et al. in prep.), some ultra-faint dwarf galaxies (Chiti et al. in prep.), and low-metallicity substructures and streams associated with them (Atzberger et al. in prep.). Our initial study serves as a powerful demonstration and validation of the utility of MAGIC photometric metallicities, to significantly enhance such studies of resolved stellar populations in the Milky Way ecosystem.

ACKNOWLEDGMENTS

Thanks to Salvatore Taibi, who kindly provided the metallicity gradient obtained with the GPR method.

This research was financed with public funds, without which it would not have been possible. This study was financed, in part, by the São Paulo Research Foundation (FAPESP), Brasil. Process Number #2022/16502-4 and #2020/15245-2. G.L. acknowledges support from KICP/UChicago through a KICP Postdoctoral Fellowship. W.C. gratefully acknowledges support from a Gruber Science Fellowship at Yale University. This material is based upon work supported by the National Science Foundation Graduate Research Fellowship Program under Grant No. DGE2139841. Any opinions, findings, and conclusions or recommendations expressed in this material are those of the author(s) and do not necessarily reflect the views of the National Science Foundation. The work of V.M.P is supported by NOIRLab, which is managed by the Association of Universities for Research in Astronomy (AURA) under a cooperative agreement with the U.S. National Science Foundation.

The DELVE project is partially supported by the NASA Fermi Guest Investigator Program Cycle 9 No. 91201. This work is partially supported by Fermilab LDRD project L2019-011. This material is based upon work supported by the National Science Foundation under Grant No. AST-2108168, AST-2108169, AST-2307126, and AST-2407526.

This project used data obtained with the Dark Energy Camera (DECam), which was constructed by the Dark Energy Survey (DES) collaboration. Funding for the DES Projects has been provided by the US Department of Energy, the U.S. National Science Foundation, the Ministry of Science and Education of Spain, the Science and Technology Facilities Council of the United Kingdom, the Higher Education Funding Council for England, the National Center for Supercomputing Applications at the University of Illinois at Urbana–Champaign, the Kavli Institute for Cosmological Physics at the University of Chicago, the Center for Cosmology and Astro-Particle Physics at the Ohio State University, the Mitchell Institute for Fundamental Physics and Astronomy at Texas A&M University, Financiadora de Estudos e Projetos, Fundação Carlos Chagas Filho de Amparo à Pesquisa do Estado do Rio de Janeiro, Conselho Nacional de Desenvolvimento Científico e Tecnológico and the Ministério da Ciência, Tecnologia e Inovação, the Deutsche Forschungsgemeinschaft and the Collaborating Institutions in the Dark Energy Survey.

The Collaborating Institutions are Argonne National Laboratory, the University of California at Santa Cruz, the University of Cambridge, Centro de Investigaciones Energéticas, Medioambientales y Tecnológicas–Madrid, the University of Chicago, University College London, the DES-Brazil Consortium, the University of Edinburgh, the Eidgenössische Technische Hochschule (ETH) Zürich, Fermi National Accelerator Laboratory, the University of Illinois at Urbana-Champaign, the Institut de Ciències de l’Espai (IEEC/CSIC), the Institut de Física d’Altes Energies, Lawrence Berkeley National Laboratory, the Ludwig-Maximilians Universität München and the associated Excellence Cluster Universe, the University of Michigan, NSF NOIRLab, the University of Nottingham, the Ohio State University, the OzDES Membership Consortium, the University of Pennsylvania, the University of Portsmouth, SLAC Na-

tional Accelerator Laboratory, Stanford University, the University of Sussex, and Texas A&M University.

Based on observations at NSF Cerro Tololo Inter-American Observatory, NSF NOIRLab (NOIRLab Prop. ID 2019A-0305; PI: Alex Drlica-Wagner, and NOIRLab Prop. ID 2023B-646244; PI: Anirudh Chiti), which is managed by the Association of Universities for Research in Astronomy (AURA) under a cooperative agreement with the U.S. National Science Foundation.

This manuscript has been authored by Fermi Research Alliance, LLC under Contract No. DE-AC02-07CH11359 with the U.S. Department of Energy, Office of Science, Office of High Energy Physics. The United States Government retains and the publisher, by accepting the article for publication, acknowledges that the United States Government retains a non-exclusive, paid-up, irrevocable, world-wide license to publish or reproduce the published form of this manuscript, or allow others to do so, for United States Government purposes.

This work has made use of data from the European Space Agency (ESA) mission *Gaia* (<https://www.cosmos.esa.int/gaia>), processed by the *Gaia* Data Processing and Analysis Consortium (DPAC, <https://www.cosmos.esa.int/web/gaia/dpac/consortium>). Funding for the DPAC has been provided by national institutions, in particular the institutions participating in the *Gaia* Multilateral Agreement.

This research made use of RStudio (RStudio Team 2020), TOPCAT (<http://www.starlink.ac.uk/topcat/>, Taylor 2005), and VizieR catalogue access tool, CDS, Strasbourg, France (Ochsenbein 1996). The original description of the VizieR service was published in Ochsenbein et al. (2000). This work also made use of NASA’s Astrophysics Data System Bibliographic Services and of the VALD database, operated at Uppsala University, the Institute of Astronomy RAS in Moscow, and the University of Vienna.

REFERENCES

- Abdurro’uf, Accetta, K., Aerts, C., et al. 2022, *ApJS*, 259, 35, doi: [10.3847/1538-4365/ac4414](https://doi.org/10.3847/1538-4365/ac4414)
- Aguado, D., Youakim, K., Hernández, J. G. G., et al. 2019, *Monthly Notices of the Royal Astronomical Society*, doi: [10.1093/mnras/stz2643](https://doi.org/10.1093/mnras/stz2643)
- Aihara, H., Arimoto, N., Armstrong, R., et al. 2018, *PASJ*, 70, S4, doi: [10.1093/pasj/psx066](https://doi.org/10.1093/pasj/psx066)
- Almeida-Fernandes, F., Placco, V. M., Rocha-Pinto, H. J., et al. 2023, *MNRAS*, 523, 2934, doi: [10.1093/mnras/stad1561](https://doi.org/10.1093/mnras/stad1561)
- Alvarez, R., & Plez, B. 1998, *A&A*, 330, 1109, doi: [10.48550/arXiv.astro-ph/9710157](https://doi.org/10.48550/arXiv.astro-ph/9710157)
- Anthony-Twarog, B. J., Heim, E. A., Twarog, B. A., & Caldwell, N. 1991, *AJ*, 102, 1056, doi: [10.1086/115932](https://doi.org/10.1086/115932)
- Arroyo-Polonio, J. M., Battaglia, G., Thomas, G. F., et al. 2024, arXiv e-prints, arXiv:2411.07283, doi: [10.48550/arXiv.2411.07283](https://doi.org/10.48550/arXiv.2411.07283)
- Barbosa, F., Chiti, A., Limberg, G., et al. 2025, The DECam MAGIC Survey: A Wide-field Photometric Metallicity Study of the Sculptor Dwarf Spheroidal Galaxy, Zenodo, doi: [10.5281/zenodo.15132837](https://doi.org/10.5281/zenodo.15132837)

- Battaglia, G., Irwin, M., Tolstoy, E., et al. 2008, *MNRAS*, 383, 183, doi: [10.1111/j.1365-2966.2007.12532.x](https://doi.org/10.1111/j.1365-2966.2007.12532.x)
- Beers, T. C., & Christlieb, N. 2005, *ARA&A*, 43, 531, doi: [10.1146/annurev.astro.42.053102.134057](https://doi.org/10.1146/annurev.astro.42.053102.134057)
- Beers, T. C., Preston, G. W., & Shectman, S. A. 1985, *AJ*, 90, 2089, doi: [10.1086/113917](https://doi.org/10.1086/113917)
- . 1992, *AJ*, 103, 1987, doi: [10.1086/116207](https://doi.org/10.1086/116207)
- Beers, T. C., Rossi, S., Norris, J. E., Ryan, S. G., & Shefler, T. 1999, *AJ*, 117, 981, doi: [10.1086/300727](https://doi.org/10.1086/300727)
- Belokurov, V. 2013, *NewAR*, 57, 100, doi: [10.1016/j.newar.2013.07.001](https://doi.org/10.1016/j.newar.2013.07.001)
- Benítez-Llambay, A., Navarro, J. F., Abadi, M. G., et al. 2016, *MNRAS*, 456, 1185, doi: [10.1093/mnras/stv2722](https://doi.org/10.1093/mnras/stv2722)
- Bettinelli, M., Hidalgo, S. L., Cassisi, S., et al. 2019, *MNRAS*, 487, 5862, doi: [10.1093/mnras/stz1679](https://doi.org/10.1093/mnras/stz1679)
- Bonifacio, P., Hill, V., Molaro, P., et al. 2000, *A&A*, 359, 663, doi: [10.48550/arXiv.astro-ph/0005268](https://doi.org/10.48550/arXiv.astro-ph/0005268)
- Bonoli, S., Marín-Franch, A., Varela, J., et al. 2021, *A&A*, 653, A31, doi: [10.1051/0004-6361/202038841](https://doi.org/10.1051/0004-6361/202038841)
- Cardona-Barrero, S., Battaglia, G., Di Cintio, A., Revaz, Y., & Jablonka, P. 2021, *MNRAS*, 505, L100, doi: [10.1093/mnras/slab059](https://doi.org/10.1093/mnras/slab059)
- Cenarro, A. J., Moles, M., Cristóbal-Hornillos, D., et al. 2019, *A&A*, 622, A176, doi: [10.1051/0004-6361/201833036](https://doi.org/10.1051/0004-6361/201833036)
- Cerny, W., Pace, A. B., Drlica-Wagner, A., et al. 2021, *ApJL*, 920, L44, doi: [10.3847/2041-8213/ac2d9a](https://doi.org/10.3847/2041-8213/ac2d9a)
- Cerny, W., Simon, J. D., Li, T. S., et al. 2023, *ApJ*, 942, 111, doi: [10.3847/1538-4357/aca1c3](https://doi.org/10.3847/1538-4357/aca1c3)
- Cerny, W., Chiti, A., Geha, M., et al. 2024, arXiv e-prints, arXiv:2410.00981, doi: [10.48550/arXiv.2410.00981](https://doi.org/10.48550/arXiv.2410.00981)
- Chiti, A., Frebel, A., Jerjen, H., Kim, D., & Norris, J. E. 2020, *ApJ*, 891, 8, doi: [10.3847/1538-4357/ab6d72](https://doi.org/10.3847/1538-4357/ab6d72)
- Chiti, A., Frebel, A., Mardini, M. K., et al. 2021, *ApJS*, 254, 31, doi: [10.3847/1538-4365/abf73d](https://doi.org/10.3847/1538-4365/abf73d)
- Chiti, A., Simon, J. D., Frebel, A., et al. 2018, *ApJ*, 856, 142, doi: [10.3847/1538-4357/aab663](https://doi.org/10.3847/1538-4357/aab663)
- Christlieb, N., Schörck, T., Frebel, A., et al. 2008, *A&A*, 484, 721, doi: [10.1051/0004-6361:20078748](https://doi.org/10.1051/0004-6361:20078748)
- Cunningham, E. C., Hunt, J. A. S., Price-Whelan, A. M., et al. 2024, *ApJ*, 963, 95, doi: [10.3847/1538-4357/ad187b](https://doi.org/10.3847/1538-4357/ad187b)
- da Costa, G., Bessell, M., Mackey, A., et al. 2019, *Monthly Notices of the Royal Astronomical Society*, doi: [10.1093/mnras/stz2550](https://doi.org/10.1093/mnras/stz2550)
- Dark Energy Survey Collaboration, Abbott, T., Abdalla, F. B., et al. 2016, *MNRAS*, 460, 1270, doi: [10.1093/mnras/stw641](https://doi.org/10.1093/mnras/stw641)
- de Boer, T. J. L., Tolstoy, E., Hill, V., et al. 2012, *A&A*, 544, A73, doi: [10.1051/0004-6361/201219547](https://doi.org/10.1051/0004-6361/201219547)
- de los Reyes, M. A. C., Kirby, E. N., Ji, A. P., & Nuñez, E. H. 2022, *ApJ*, 925, 66, doi: [10.3847/1538-4357/ac332b](https://doi.org/10.3847/1538-4357/ac332b)
- Deason, A. J., & Belokurov, V. 2024, *NewAR*, 99, 101706, doi: [10.1016/j.newar.2024.101706](https://doi.org/10.1016/j.newar.2024.101706)
- Dey, A., Schlegel, D. J., Lang, D., et al. 2019, *AJ*, 157, 168, doi: [10.3847/1538-3881/ab089d](https://doi.org/10.3847/1538-3881/ab089d)
- Dotter, A., Chaboyer, B., Jevremović, D., et al. 2008, *ApJS*, 178, 89, doi: [10.1086/589654](https://doi.org/10.1086/589654)
- Drlica-Wagner, A., Carlin, J. L., Nidever, D. L., et al. 2021, *ApJS*, 256, 2, doi: [10.3847/1538-4365/ac079d](https://doi.org/10.3847/1538-4365/ac079d)
- Drlica-Wagner, A., Ferguson, P. S., Adamów, M., et al. 2022, *ApJS*, 261, 38, doi: [10.3847/1538-4365/ac78eb](https://doi.org/10.3847/1538-4365/ac78eb)
- El-Badry, K., Wetzel, A., Geha, M., et al. 2016, *ApJ*, 820, 131, doi: [10.3847/0004-637X/820/2/131](https://doi.org/10.3847/0004-637X/820/2/131)
- Faber, S. M., & Gallagher, J. S. 1979, *ARA&A*, 17, 135, doi: [10.1146/annurev.aa.17.090179.001031](https://doi.org/10.1146/annurev.aa.17.090179.001031)
- Faber, S. M., Phillips, A. C., Kibrick, R. I., et al. 2003, in *Society of Photo-Optical Instrumentation Engineers (SPIE) Conference Series*, Vol. 4841, Instrument Design and Performance for Optical/Infrared Ground-based Telescopes, ed. M. Iye & A. F. M. Moorwood, 1657–1669, doi: [10.1117/12.460346](https://doi.org/10.1117/12.460346)
- Flaugher, B., Diehl, H. T., Honscheid, K., et al. 2015, *AJ*, 150, 150, doi: [10.1088/0004-6256/150/5/150](https://doi.org/10.1088/0004-6256/150/5/150)
- Frebel, A., Christlieb, N., Norris, J. E., et al. 2006, *ApJ*, 652, 1585, doi: [10.1086/508506](https://doi.org/10.1086/508506)
- Fu, S. W., Weisz, D. R., Starkenburg, E., et al. 2022, *ApJ*, 925, 6, doi: [10.3847/1538-4357/ac3665](https://doi.org/10.3847/1538-4357/ac3665)
- . 2023, *ApJ*, 958, 167, doi: [10.3847/1538-4357/ad0030](https://doi.org/10.3847/1538-4357/ad0030)
- . 2024a, *ApJ*, 965, 36, doi: [10.3847/1538-4357/ad25ed](https://doi.org/10.3847/1538-4357/ad25ed)
- . 2024b, *ApJ*, 975, 2, doi: [10.3847/1538-4357/ad76a2](https://doi.org/10.3847/1538-4357/ad76a2)
- Gaia Collaboration, Prusti, T., de Bruijne, J. H. J., et al. 2016, *A&A*, 595, A1, doi: [10.1051/0004-6361/201629272](https://doi.org/10.1051/0004-6361/201629272)
- Gaia Collaboration, Brown, A. G. A., Vallenari, A., et al. 2021, *A&A*, 649, A1, doi: [10.1051/0004-6361/202039657](https://doi.org/10.1051/0004-6361/202039657)
- Gaia Collaboration, Vallenari, A., Brown, A. G. A., et al. 2023, *A&A*, 674, A1, doi: [10.1051/0004-6361/202243940](https://doi.org/10.1051/0004-6361/202243940)
- Gustafsson, B., Edvardsson, B., Eriksson, K., et al. 2008, *A&A*, 486, 951, doi: [10.1051/0004-6361:200809724](https://doi.org/10.1051/0004-6361:200809724)
- Han, S.-I., Kim, H.-S., Yoon, S.-J., et al. 2020, *ApJS*, 247, 7, doi: [10.3847/1538-4365/ab6441](https://doi.org/10.3847/1538-4365/ab6441)
- Helmi, A. 2008, *A&A Rv*, 15, 145, doi: [10.1007/s00159-008-0009-6](https://doi.org/10.1007/s00159-008-0009-6)
- . 2020, *ARA&A*, 58, 205, doi: [10.1146/annurev-astro-032620-021917](https://doi.org/10.1146/annurev-astro-032620-021917)
- Hill, V., Skúladóttir, Á., Tolstoy, E., et al. 2019, *A&A*, 626, A15, doi: [10.1051/0004-6361/201833950](https://doi.org/10.1051/0004-6361/201833950)
- Ho, N., Geha, M., Tollerud, E. J., et al. 2015, *ApJ*, 798, 77, doi: [10.1088/0004-637X/798/2/77](https://doi.org/10.1088/0004-637X/798/2/77)

- Howell, M., Campbell, S. W., Stello, D., & De Silva, G. M. 2024, *MNRAS*, 527, 7974, doi: [10.1093/mnras/stad3565](https://doi.org/10.1093/mnras/stad3565)
- Huang, Y., Beers, T. C., Wolf, C., et al. 2022, *ApJ*, 925, 164, doi: [10.3847/1538-4357/ac21cb](https://doi.org/10.3847/1538-4357/ac21cb)
- Johnston, K. V. 1998, *ApJ*, 495, 297, doi: [10.1086/305273](https://doi.org/10.1086/305273)
- Kauffmann, G., White, S. D. M., & Guiderdoni, B. 1993, *MNRAS*, 264, 201, doi: [10.1093/mnras/264.1.201](https://doi.org/10.1093/mnras/264.1.201)
- Keller, S. C., Schmidt, B. P., Bessell, M. S., et al. 2007, *Publications of the Astronomical Society of Australia*, 24, 1–12, doi: [10.1071/AS07001](https://doi.org/10.1071/AS07001)
- Keller, S. C., Bessell, M. S., Frebel, A., et al. 2014, *Nature*, 506, 463, doi: [10.1038/nature12990](https://doi.org/10.1038/nature12990)
- Kennicutt, Jr., R. C. 1983, *ApJ*, 272, 54, doi: [10.1086/161261](https://doi.org/10.1086/161261)
- Kirby, E. N., Cohen, J. G., Guhathakurta, P., et al. 2013, *ApJ*, 779, 102, doi: [10.1088/0004-637X/779/2/102](https://doi.org/10.1088/0004-637X/779/2/102)
- Kirby, E. N., Guhathakurta, P., Bolte, M., Sneden, C., & Geha, M. C. 2009, *ApJ*, 705, 328, doi: [10.1088/0004-637X/705/1/328](https://doi.org/10.1088/0004-637X/705/1/328)
- Kirby, E. N., Lanfranchi, G. A., Simon, J. D., Cohen, J. G., & Guhathakurta, P. 2011, *ApJ*, 727, 78, doi: [10.1088/0004-637X/727/2/78](https://doi.org/10.1088/0004-637X/727/2/78)
- Kirby, E. N., Guhathakurta, P., Simon, J. D., et al. 2010, *ApJS*, 191, 352, doi: [10.1088/0067-0049/191/2/352](https://doi.org/10.1088/0067-0049/191/2/352)
- Kirby, E. N., Guo, M., Zhang, A. J., et al. 2015, *ApJ*, 801, 125, doi: [10.1088/0004-637X/801/2/125](https://doi.org/10.1088/0004-637X/801/2/125)
- Koch, A., Grebel, E. K., Gilmore, G. F., et al. 2008, *AJ*, 135, 1580, doi: [10.1088/0004-6256/135/4/1580](https://doi.org/10.1088/0004-6256/135/4/1580)
- Lai, D. K., Lee, Y. S., Bolte, M., et al. 2011, *ApJ*, 738, 51, doi: [10.1088/0004-637X/738/1/51](https://doi.org/10.1088/0004-637X/738/1/51)
- Lardo, C., Battaglia, G., Pancino, E., et al. 2016, *A&A*, 585, A70, doi: [10.1051/0004-6361/201527391](https://doi.org/10.1051/0004-6361/201527391)
- Leaman, R., Venn, K. A., Brooks, A. M., et al. 2013, *ApJ*, 767, 131, doi: [10.1088/0004-637X/767/2/131](https://doi.org/10.1088/0004-637X/767/2/131)
- Limberg, G., Rossi, S., Beers, T. C., et al. 2021, *ApJ*, 907, 10, doi: [10.3847/1538-4357/abcb87](https://doi.org/10.3847/1538-4357/abcb87)
- Limberg, G., Queiroz, A. B. A., Perottoni, H. D., et al. 2023, *ApJ*, 946, 66, doi: [10.3847/1538-4357/acb694](https://doi.org/10.3847/1538-4357/acb694)
- Longeard, N., Martin, N., Starkenburg, E., et al. 2018, *MNRAS*, 480, 2609, doi: [10.1093/mnras/sty1986](https://doi.org/10.1093/mnras/sty1986)
- . 2020, *MNRAS*, 491, 356, doi: [10.1093/mnras/stz2854](https://doi.org/10.1093/mnras/stz2854)
- Longeard, N., Jablonka, P., Arentsen, A., et al. 2022, *MNRAS*, 516, 2348, doi: [10.1093/mnras/stac1827](https://doi.org/10.1093/mnras/stac1827)
- Majewski, S. R., Skrutskie, M. F., Weinberg, M. D., & Ostheimer, J. C. 2003, *ApJ*, 599, 1082, doi: [10.1086/379504](https://doi.org/10.1086/379504)
- Martin, N. F., Starkenburg, E., Yuan, Z., et al. 2024, *A&A*, 692, A115, doi: [10.1051/0004-6361/202347633](https://doi.org/10.1051/0004-6361/202347633)
- Martínez-Vázquez, C. E., Monelli, M., Bono, G., et al. 2015, *MNRAS*, 454, 1509, doi: [10.1093/mnras/stv2014](https://doi.org/10.1093/mnras/stv2014)
- Martínez-Vázquez, C. E., Monelli, M., Gallart, C., et al. 2016, *MNRAS*, 461, L41, doi: [10.1093/mnrasl/slw093](https://doi.org/10.1093/mnrasl/slw093)
- Mau, S., Cerny, W., Pace, A. B., et al. 2020, *ApJ*, 890, 136, doi: [10.3847/1538-4357/ab6c67](https://doi.org/10.3847/1538-4357/ab6c67)
- McConnachie, A. W. 2012, *AJ*, 144, 4, doi: [10.1088/0004-6256/144/1/4](https://doi.org/10.1088/0004-6256/144/1/4)
- Mendes de Oliveira, C., Ribeiro, T., Schoenell, W., et al. 2019, *MNRAS*, 489, 241, doi: [10.1093/mnras/stz1985](https://doi.org/10.1093/mnras/stz1985)
- Mercado, F. J., Bullock, J. S., Boylan-Kolchin, M., et al. 2021, *MNRAS*, 501, 5121, doi: [10.1093/mnras/staa3958](https://doi.org/10.1093/mnras/staa3958)
- Monaco, L., Bellazzini, M., Bonifacio, P., et al. 2005, *A&A*, 441, 141, doi: [10.1051/0004-6361:20053333](https://doi.org/10.1051/0004-6361:20053333)
- Muñoz, R. R., Côté, P., Santana, F. A., et al. 2018, *ApJ*, 860, 66, doi: [10.3847/1538-4357/aac16b](https://doi.org/10.3847/1538-4357/aac16b)
- Mucciarelli, A., Bellazzini, M., & Massari, D. 2021, *A&A*, 653, A90, doi: [10.1051/0004-6361/202140979](https://doi.org/10.1051/0004-6361/202140979)
- Muggeo, V. M. 2003, *Statistics in Medicine*, 22, 3055
- Ochsenbein, F. 1996, *The VizieR database of astronomical catalogues*, CDS, Centre de Données astronomiques de Strasbourg, doi: [10.26093/CDS/VIZIER](https://doi.org/10.26093/CDS/VIZIER)
- Ochsenbein, F., Bauer, P., & Marcout, J. 2000, *A&AS*, 143, 23, doi: [10.1051/aas:2000169](https://doi.org/10.1051/aas:2000169)
- Pace, A. B. 2024, arXiv e-prints, arXiv:2411.07424, doi: [10.48550/arXiv.2411.07424](https://doi.org/10.48550/arXiv.2411.07424)
- Pace, A. B., Erkal, D., & Li, T. S. 2022, *ApJ*, 940, 136, doi: [10.3847/1538-4357/ac997b](https://doi.org/10.3847/1538-4357/ac997b)
- Pace, A. B., Kaplinghat, M., Kirby, E., et al. 2020, *MNRAS*, 495, 3022, doi: [10.1093/mnras/staa1419](https://doi.org/10.1093/mnras/staa1419)
- Pan, Y., Chiti, A., Drlica-Wagner, A., et al. 2025, *ApJ*, 978, 39, doi: [10.3847/1538-4357/ad9820](https://doi.org/10.3847/1538-4357/ad9820)
- Pietrinferni, A., Cassisi, S., Salaris, M., & Castelli, F. 2004, *ApJ*, 612, 168, doi: [10.1086/422498](https://doi.org/10.1086/422498)
- Piskunov, N. E., Kupka, F., Ryabchikova, T. A., Weiss, W. W., & Jeffery, C. S. 1995, *A&AS*, 112, 525
- Placco, V. M., Almeida-Fernandes, F., Arentsen, A., et al. 2022, *ApJS*, 262, 8, doi: [10.3847/1538-4365/ac7ab0](https://doi.org/10.3847/1538-4365/ac7ab0)
- Plez, B. 2012, *Turbospectrum: Code for spectral synthesis*, *Astrophysics Source Code Library*, record ascl:1205.004
- Reichert, M., Hansen, C. J., Hanke, M., et al. 2020, *A&A*, 641, A127, doi: [10.1051/0004-6361/201936930](https://doi.org/10.1051/0004-6361/201936930)
- Revaz, Y., & Jablonka, P. 2018, *A&A*, 616, A96, doi: [10.1051/0004-6361/201832669](https://doi.org/10.1051/0004-6361/201832669)
- Riello, M., De Angeli, F., Evans, D. W., et al. 2021, *A&A*, 649, A3, doi: [10.1051/0004-6361/202039587](https://doi.org/10.1051/0004-6361/202039587)
- Ross, T. L., Holtzman, J., Saha, A., & Anthony-Twarog, B. J. 2015, *AJ*, 149, 198, doi: [10.1088/0004-6256/149/6/198](https://doi.org/10.1088/0004-6256/149/6/198)
- RStudio Team. 2020, *RStudio: Integrated Development Environment for R*, RStudio, PBC., Boston, MA. <http://www.rstudio.com/>

- Ryabchikova, T., Piskunov, N., Kurucz, R. L., et al. 2015, *PhyS*, 90, 054005, doi: [10.1088/0031-8949/90/5/054005](https://doi.org/10.1088/0031-8949/90/5/054005)
- Sandford, N. R., Weinberg, D. H., Weisz, D. R., & Fu, S. W. 2024, *MNRAS*, 530, 2315, doi: [10.1093/mnras/stae1010](https://doi.org/10.1093/mnras/stae1010)
- Savino, A., de Boer, T. J. L., Salaris, M., & Tolstoy, E. 2018, *MNRAS*, 480, 1587, doi: [10.1093/mnras/sty1954](https://doi.org/10.1093/mnras/sty1954)
- Schlegel, D. J., Finkbeiner, D. P., & Davis, M. 1998, *ApJ*, 500, 525, doi: [10.1086/305772](https://doi.org/10.1086/305772)
- Schroyen, J., De Rijcke, S., Koleva, M., Cloet-Osselaer, A., & Vandenbroucke, B. 2013, *MNRAS*, 434, 888, doi: [10.1093/mnras/stt1084](https://doi.org/10.1093/mnras/stt1084)
- Searle, L., & Zinn, R. 1978, *ApJ*, 225, 357, doi: [10.1086/156499](https://doi.org/10.1086/156499)
- Sestito, F., Roediger, J., Navarro, J. F., et al. 2023, *MNRAS*, 523, 123, doi: [10.1093/mnras/stad1417](https://doi.org/10.1093/mnras/stad1417)
- Shetrone, M. D., Côté, P., & Sargent, W. L. W. 2001, *ApJ*, 548, 592, doi: [10.1086/319022](https://doi.org/10.1086/319022)
- Simon, J. D., Jacobson, H. R., Frebel, A., et al. 2015, *ApJ*, 802, 93, doi: [10.1088/0004-637X/802/2/93](https://doi.org/10.1088/0004-637X/802/2/93)
- Springel, V., Frenk, C. S., & White, S. D. M. 2006, *Nature*, 440, 1137, doi: [10.1038/nature04805](https://doi.org/10.1038/nature04805)
- Starkenbourg, E., Martin, N., Youakim, K., et al. 2017, *MNRAS*, 471, 2587, doi: [10.1093/mnras/stx1068](https://doi.org/10.1093/mnras/stx1068)
- Taibi, S., Battaglia, G., Leaman, R., et al. 2022, *A&A*, 665, A92, doi: [10.1051/0004-6361/202243508](https://doi.org/10.1051/0004-6361/202243508)
- Tan, C. Y., Cerny, W., Drlica-Wagner, A., et al. 2024, arXiv e-prints, arXiv:2408.00865, doi: [10.48550/arXiv.2408.00865](https://doi.org/10.48550/arXiv.2408.00865)
- Tang, B., Zhang, J., Yan, Z., et al. 2023, *A&A*, 669, A125, doi: [10.1051/0004-6361/202244052](https://doi.org/10.1051/0004-6361/202244052)
- Taylor, M. B. 2005, in *Astronomical Society of the Pacific Conference Series*, Vol. 347, *Astronomical Data Analysis Software and Systems XIV*, ed. P. Shopbell, M. Britton, & R. Ebert, 29
- Tolstoy, E., Irwin, M. J., Helmi, A., et al. 2004, *ApJL*, 617, L119, doi: [10.1086/427388](https://doi.org/10.1086/427388)
- Tolstoy, E., Hill, V., Irwin, M., et al. 2006, *The Messenger*, 123, 33
- Tolstoy, E., Skúladóttir, Á., Battaglia, G., et al. 2023, *A&A*, 675, A49, doi: [10.1051/0004-6361/202245717](https://doi.org/10.1051/0004-6361/202245717)
- Ural, U., Wilkinson, M. I., Koch, A., et al. 2010, *MNRAS*, 402, 1357, doi: [10.1111/j.1365-2966.2009.15975.x](https://doi.org/10.1111/j.1365-2966.2009.15975.x)
- Vincenzo, F., Matteucci, F., de Boer, T. J. L., Cignoni, M., & Tosi, M. 2016, *MNRAS*, 460, 2238, doi: [10.1093/mnras/stw1145](https://doi.org/10.1093/mnras/stw1145)
- Virtanen, P., Gommers, R., Oliphant, T. E., et al. 2020, *Nature Methods*, 17, 261, doi: [10.1038/s41592-019-0686-2](https://doi.org/10.1038/s41592-019-0686-2)
- Vitali, S., Arentsen, A., Starkenburg, E., et al. 2022, *MNRAS*, 517, 6121, doi: [10.1093/mnras/stac2869](https://doi.org/10.1093/mnras/stac2869)
- Walker, M. G., Caldwell, N., Mateo, M., et al. 2023, *ApJS*, 268, 19, doi: [10.3847/1538-4365/acdd79](https://doi.org/10.3847/1538-4365/acdd79)
- Walker, M. G., Mateo, M., & Olszewski, E. W. 2009, *AJ*, 137, 3100, doi: [10.1088/0004-6256/137/2/3100](https://doi.org/10.1088/0004-6256/137/2/3100)
- Weinberg, D. H., Andrews, B. H., & Freudenburg, J. 2017, *ApJ*, 837, 183, doi: [10.3847/1538-4357/837/2/183](https://doi.org/10.3847/1538-4357/837/2/183)
- Weisz, D. R., Dolphin, A. E., Skillman, E. D., et al. 2014, *ApJ*, 789, 147, doi: [10.1088/0004-637X/789/2/147](https://doi.org/10.1088/0004-637X/789/2/147)
- White, S. D. M., & Frenk, C. S. 1991, *ApJ*, 379, 52, doi: [10.1086/170483](https://doi.org/10.1086/170483)
- Willmer, C. N. A. 2018, *ApJS*, 236, 47, doi: [10.3847/1538-4365/aabfdf](https://doi.org/10.3847/1538-4365/aabfdf)
- Yong, D., Costa, G., Bessell, M., et al. 2021, *Monthly Notices of the Royal Astronomical Society*, doi: [10.1093/mnras/stab2001](https://doi.org/10.1093/mnras/stab2001)
- Youakim, K., Starkenburg, E., Aguado, D. S., et al. 2017, *MNRAS*, 472, 2963, doi: [10.1093/mnras/stx2005](https://doi.org/10.1093/mnras/stx2005)

Facilities: Blanco (DECam), Astro Data Lab, Gaia

Software: RStudio (RStudio Team 2020), Scipy (Virtanen et al. 2020), TOPCAT (Taylor 2005)

APPENDIX

A. COMPARISON WITH SPECTROSCOPIC WORKS

In Table 2, we compile the median values and offsets obtained comparing MAGIC estimates to previous datasets. The Chiti et al. (2018) study gives the worst comparison to the photometric metallicities, since their sample generally includes lower metallicity stars that are more carbon-enhanced. As mentioned in Section 4, the accuracy of photometric $[\text{Fe}/\text{H}]$ decreases to more metal-poor stars and carbon enhancement can also affect the estimates. In addition to $[\text{Fe}/\text{H}]$, we included $[\text{Ca}/\text{H}]$ values from R22, since the MAGIC metallicities are derived from flux measured in the Ca H and K lines. Although the median values agree better with a similar offset, the distribution observed for $[\text{Ca}/\text{H}]$ is not consistent with the MDF presented in Section 5.1.

Table 2. Comparison of MAGIC data with spectroscopic samples. For each work, the number of stars in common (N) and the median values using the spectroscopic ($[\text{Fe}/\text{H}]_{\text{spec}}$) and photometric ($[\text{Fe}/\text{H}]_{\text{MAGIC}}$) estimates are presented. The median values of $\Delta[\text{Fe}/\text{H}]$ are also provided ($M_{\Delta[\text{Fe}/\text{H}]}$).

| Work | N | $[\text{Fe}/\text{H}]_{\text{spec}}$ | $[\text{Fe}/\text{H}]_{\text{MAGIC}}$ | $M_{\Delta[\text{Fe}/\text{H}]}$ |
|---|------|--------------------------------------|---------------------------------------|----------------------------------|
| Tolstoy et al. (2023) | 1148 | -1.82 | -1.81 | -0.02 |
| Walker et al. (2023) | 194 | -1.59 | -1.72 | -0.14 |
| de los Reyes et al. (2022) – $[\text{Fe}/\text{H}]$ | 366 | -1.66 | -1.53 | 0.09 |
| de los Reyes et al. (2022) – $[\text{Ca}/\text{H}]$ | 350 | -1.50 | -1.53 | -0.10 |
| Reichert et al. (2020) | 77 | -1.56 | -1.61 | -0.11 |
| Hill et al. (2019) | 76 | -1.57 | -1.60 | -0.03 |
| Chiti et al. (2018) | 64 | -2.84 | -2.35 | 0.38 |
| Kirby et al. (2009) | 328 | -1.58 | -1.52 | 0.03 |
| APOGEE DR17 | 147 | -1.69 | -1.88 | -0.16 |

B. DATA AVAILABILITY

The catalog for Scl dSph members analyzed in this work is available at the following Zenodo DOI: [10.5281/zenodo.15132837](https://doi.org/10.5281/zenodo.15132837) (Barbosa et al. 2025). It presents both Gaia and DELVE photometry, membership probabilities from Pace et al. (2022), and stellar parameters ($\log g$ and $[\text{Fe}/\text{H}]$) derived following the method described in Section 3.1. A fragment of the full online sample is presented in Table 3.

Table 3. Scl dSph member analyzed in this work. Gaia source_id, right ascension (ra), declination (dec), and G magnitude are provided. Photometry from DELVE DR2 (g -, r -, and i -band) are available, as well as derived $\log g$ and $[\text{Fe}/\text{H}]$.

| source_id | ra | dec | phot_g_mean_mag | g_dered | r_dered | i_dered | logg_magic | feh_magic |
|---------------------|--------|---------|-----------------|---------|---------|---------|------------|-----------|
| 5003194866102866048 | 15.006 | -33.855 | 17.470 | 18.157 | 17.368 | 17.064 | 1.326 | -2.153 |
| 5003199775249111680 | 14.955 | -33.735 | 17.762 | 18.420 | 17.628 | 17.324 | 1.399 | -1.527 |
| 5027218267457408384 | 15.031 | -33.722 | 17.249 | 17.989 | 17.102 | 16.775 | 1.173 | -1.891 |
| 5027219126450866816 | 15.010 | -33.688 | 18.059 | 18.729 | 17.917 | 17.637 | 1.539 | -1.126 |
| 5027219779285852672 | 15.009 | -33.655 | 18.103 | 18.708 | 17.974 | 17.709 | 1.572 | -1.595 |